

# Electronic Supplementary Information

for

## Side-chain tuning in conjugated polymer photocatalysts for improved hydrogen production from water

Duncan J. Woods,<sup>a,‡</sup> Sam A. J. Hillman,<sup>b,‡</sup> Drew Pearce,<sup>b</sup> Liam Wilbraham,<sup>c</sup> Lucas Q. Flagg,<sup>d</sup> Warren Duffy,<sup>e</sup> Iain McCulloch,<sup>e</sup> James R. Durrant,<sup>f</sup> Anne A. Y. Guilbert,<sup>b</sup> Martijn A. Zwijnenburg,<sup>c,\*</sup> Reiner Sebastian Sprick,<sup>a,\*</sup> Jenny Nelson,<sup>b,\*</sup> and Andrew I. Cooper<sup>a,\*</sup>

<sup>a</sup> Department of Chemistry and Material Innovation Factory, University of Liverpool, Crown Street, Liverpool L69 7ZD, UK.

<sup>b</sup> Department of Physics and Centre for Plastic Electronics, Imperial College London, Prince Consort Road, London SW7 2AZ, UK.

<sup>c</sup> Department of Chemistry, University College London, 20 Gordon Street, London WC1H 0AJ, UK.

<sup>d</sup> Department of Chemistry, University of Washington, Seattle WA 98195-1700, USA.

<sup>e</sup> King Abdullah University of Science and Technology, KAUST Solar Center, Thuwal 23955, Saudi Arabia.

<sup>f</sup> Department of Chemistry and Centre for Plastic Electronics, Imperial College London, Exhibition Road, London SW7 2AZ, UK.

<sup>‡</sup> These authors contributed equally.

**General methods.** All reagents were obtained from Sigma-Aldrich, or Fluorochem and used as received, except for 2,7-dibromo-9,9-bis[2-[2-(2-methoxyethoxy)ethoxy]ethyl]-9H-fluorene,<sup>1</sup> 3,7-dibromodibenzo[*b,d*]thiophene sulfone,<sup>2</sup> **FP-Me**<sup>2</sup> and **FS-Me**<sup>3</sup> which were synthesized using previously reported procedures. Reactions were carried out under nitrogen atmosphere using standard Schlenk techniques. Solution <sup>1</sup>H NMR spectra were recorded at 400.13 MHz on a Bruker Avance 400 NMR spectrometer. CHN Analysis was performed on a Thermo EA1112 Flash CHNS-O Analyzer using standard microanalytical procedures. Palladium content was determined *via* ICP-MS analysis performed on a Perkin Elmer ICP MS NexION 2000 with equipped with a collision/reaction cell after a microwave digest of the materials in nitric acid (67-69%, trace metal analysis grade) in a microwave. The solutions were diluted with water before the measurement and the instrument was calibrated with Pd standards in aqueous solution and Ge-74 as the internal standard. The mass peak at 106 m/z with He KED mode was used to calculate the amount of residual palladium in the samples. ICP-OES by Butterworth Laboratories Ltd (Teddington, United Kingdom) was used to determine Pd content in the case of FS-Oct. PXRD measurements were performed on a Panalytical Empyrean diffractometer, with a Cu X-ray source ( $\lambda = 1.5418 \text{ \AA}$ , Cu-K $\alpha$ ), used in high throughput transmission mode with K $\alpha$  focusing mirror and PIXcel 3D detector. Gel permeation chromatography was performed using an Agilent 1260 Infinity II GPC/SEC system equipped with two PLgel 5  $\mu\text{m}$  MIXED-D columns and a PLgel 5  $\mu\text{m}$  guard column and refractive index detector. Chloroform was used as the mobile phase with a flow-rate of 1 mL min<sup>-1</sup> at 40 °C. GPC data was analyzed using Agilent software and Agilent EasiCal PS-2 standards were used. Thermogravimetric analysis was performed on an EXSTAR6000 by heating samples at 10 °C min<sup>-1</sup> under air in open aluminium pans to 600 °C. Imaging of the polymer morphology was performed on a Hitachi S4800 Cold Field Emission SEM, with secondary electron, backscatter and transmission detectors. Contact angle measurements were performed using a Krüss DSA100 instrument on films of all soluble polymers drop-cast from chloroform onto glass microscope slides and a pellet of insoluble **FS-Me** and **FP-Me**. The Laplace-Young method was used to calculate contact angles of 5  $\mu\text{L}$  droplets of water over the course of eleven frames taken over ten seconds at three different positions on the cast films.

UV-Visible absorption spectra of polymers were calculated from either transmittance (thin films and solutions in chloroform) or reflectance (solid-state) measurements using a Shimadzu UV-2550 UV-Vis spectrometer. Photoluminescence spectra of the polymers as

powders, thin films and in chloroform solutions were measured on a Shimadzu RF-5301PC fluorescence spectrometer. Photoluminescence spectra of dispersions in water/methanol/TEA were taken using a FLS1000 PL spectrometer (Edinburgh Instruments).

Water vapor isotherms were determined at 293 K using an IGA gravimetric adsorption apparatus (Hiden Isochema, U.K.) with anti-condensation system, which was carried out in an ultrahigh vacuum system equipped with a diaphragm and turbo pumps. All AFM images were taken on an Asylum Research Cypher-ES instrument. Dry thickness measurements were taken by imaging across a razor blade scratch in tapping mode using 75 kHz HQ:NSC18/Pt tips (MikroMasch). Swollen measurements were then taken by depositing 100  $\mu$ l of solvent (Milli-Q water or TEA) onto the sample and imaging the same area of the film in contact mode using ContGB-G tips (BudgetSensors). All AFM measurements were taken in an N<sub>2</sub> flow cell. QCM measurements were performed using a QCM200 (Stanford Research Systems) on 5 MHz gold-coated AT quartz crystals. Prior to polymer deposition, each crystal's steady-state frequency was measured in both air and water. After spin coating the polymer, the new steady-state frequency in both air and water was recorded. Signals were recorded using a potentiostat (MetroOhm Autolab PGSTAT204). Static light scattering measurements were performed on a Malvern Mastersizer 3000 Particle Sizer; polymers were dispersed in water and water/methanol/triethylamine (1:1:1) mixtures by sonication for 40 minutes. The resultant suspensions were injected into a stirred Hydro SV quartz cell, containing more of the requisite medium to give a laser obscuration of 5 – 10%. Particle sizes were fitted according to Mie theory, using the Malvern 'General Purpose' analysis model, for non-spherical particles with fine powder mode turned on. A polymer refractive index of 1.59, polymer absorbance of 0.1 and solvent refractive indices of 1.330 and 1.353 were used for fitting for the respective media.

Photoelectron spectroscopy in air (PESA) measurements were recorded using a Riken Keiki PESA spectrometer (Model AC-2). Samples for PESA were prepared on glass substrates. All spectroelectrochemical measurements were performed using a three-electrode setup comprising an 0.1 molar tetrabutylammonium hexafluorophosphate electrolyte in acetonitrile, an Ag/AgCl reference electrode ( $E^0 = +0.22$  V vs SHE), a platinum mesh counter electrode and a homemade PEEK cell with quartz windows. The working electrode was made from polymer films spincoated onto *n*-octyltrichlorosilane-coated substrates, which in themselves comprised a layer of either indium- or fluorine-doped tin oxide on glass. The electrolyte was degassed with argon both for 20 minutes prior to measurements beginning and also during the

measurements themselves. Absorbance spectra were measured using a tungsten lamp probe beam and an OceanOptics USB 2000+ UV-vis spectrometer. Films were illuminated from the front (i.e. not through the substrate) during absorption measurements. Potentials were applied to the working electrode using an Ivium CompactStat potentiostat at a scan rate of 100 mVs<sup>-1</sup>, starting at 0 V vs Ag/AgCl.

Cyclic voltammetry measurements were also made in a standard 3-electrode cell with a platinum wire counter electrode and an Ag/AgCl reference electrode (saturated LiCl in ethanol, E=0.143 V versus SHE). The polymer was deposited on ITO-coated glass slides as the working electrode. The solvent was acetonitrile with a 0.1 M tetrabutylammonium hexafluorophosphate supporting electrolyte. The ionization potential was calculated by extrapolating the onset of the oxidative current to the current baseline (intercept of red lines). The potential was converted to the vacuum scale using the following equation:

$$E_{vacuum} = - (E_{Ag/AgCl} + E_{SHE}^{Ag/AgCl} + 4.44)$$

where the terms on the right-hand side are the measured ionization potential versus Ag/AgCl, the potential of the reference electrode versus the standard hydrogen electrode (SHE) and the potential of the SHE versus vacuum, respectively.

**Theoretical calculations.** The ionization potential and electron affinity associated with the charge carriers (IP/EA) and excitons (IP\*/EA\*) were calculated using our standard approach<sup>4</sup> based around (time-dependent) density functional theory ((TD-)DFT) calculations. These (TD-)DFT calculations used the B3LYP density functional<sup>5-7</sup> and the DZP basis-set,<sup>8</sup> as well as the COSMO solvation model<sup>9</sup> with  $\epsilon_r = 80.1$  (water), 2.38 (TEA) and 2.0 (dry polymer) used to describe the environment around the polymer backbone. The absorption onset of the polymers was calculated using the same set-up, except that while for the calculation of the exciton potentials the Tamm-Dancoff approximation<sup>10</sup> is made this approximation is omitted here. All (TD-)DFT calculations were performed using Turbomole 7.1.<sup>11,12</sup> Potentials of the solution reactions were taken from previous work.<sup>12</sup> Here protons were modelled as adducts with TEA (e.g.  $2 \text{ TEA}:\text{H}^+ + 2 \text{ e}^- \rightarrow \text{H}_2 + 2 \text{ TEA}$ ), which allows us to predict potentials in both water and TEA on an equal footing.

**Transient absorption measurements.** Microsecond<sup>13</sup> and femtosecond<sup>14</sup> transient absorption spectroscopy (TAS) experiments were performed in transmission mode using in-house setups described previously. Dispersions of each polymer in different liquid environments were excited using 420 nm light, matching the cut-off wavelength used in hydrogen evolution experiments. Ground state transmission spectra for all TAS samples were taken using an Agilent Cary 60 UV-Vis spectrophotometer and converted to absorption data using a cuvette of the appropriate solvent as a reference. Scattering was neglected in these calculations.

The excitation source for microsecond TAS experiments was a Nd:YAG laser (Opolette 355 II, 7 ns pulse width) with an optical parametric oscillator used to achieve the 420 nm excitation wavelength. Samples were made at a concentration of 0.02 mg mL<sup>-1</sup> in 10 mm quartz cuvettes (Hellma Analytics). Unless otherwise stated, these were excited at a fluence of 1.5 mJ cm<sup>-2</sup> with kinetic traces taken over 100-500 individual excitation pulses generated at a frequency of 1.0 Hz.

Femtosecond TAS samples were made at a concentration of 0.2 mg mL<sup>-1</sup> in 2 mm quartz cuvettes (Hellma Analytics) unless otherwise stated. Fs-TAS measurements were made using a regeneratively amplified Ti:sapphire laser (Solstice, Spectra-Physics) combined with Helios spectrometers (Ultrafast Systems). The 800 nm output was then converted to the final 420 nm excitation beam using an optical parametric amplifier (TOPAS Prime, Spectra-Physics) and a frequency mixer (NirUVis, Light Conversion). Some data in the SI were measured using 355 nm excitation. Transient transmission spectra were probed in the visible spectrum by adjusting the referenced setup such that the amplifier output was focussed into a Ti:sapphire crystal which produces a continuum in the 460-740 nm range. Unless otherwise stated, the excitation fluence was 87 μJ cm<sup>-2</sup>. The excitation repetition rate was 500 Hz and each delay time was averaged over two seconds. Transmission spectra were averaged over a minimum of 4 sequential two-second measurements depending on the amplitude of the optical response. Group velocity dispersion was corrected using the software Surface Explorer 4.2 (Ultrafast Systems).

Deconvoluted 600 nm kinetics were calculated as follows: The TA spectrum observed at 0.5 ps after excitation was assumed to only contain spectral contributions from stimulated/spontaneous emission (negative, around 500 nm) and exciton absorption

(positive, around 700 nm). This is long enough after excitation to avoid instrument response effects but too early to include any significant contributions from charge formation. For all spectra beyond 0.5 ps (individually “the spectrum of interest”), the 0.5 ps spectrum was scaled such that its absorption amplitude at 725 nm matched the 725 nm absorption amplitude of the spectrum of interest. The scaled 0.5 ps spectrum therefore gives both the shape and the absorption amplitude of all non-polaronic states; by subtracting each scaled 0.5 ps spectrum from each spectrum of interest, the absorption contribution of generated polarons was obtained for each time. This absorption contribution peaked in the 600 nm region. By combining all spectra together, the kinetics of the electron polaron were extracted.

**Filtration study.** Due to the high polydispersity of the samples in this work, light scattering measurements were considered unsuitable for probing the sizes of the smallest particles, which are the ones that have the highest specific photocatalytic activity. Instead, **Figure S-25** comprises a diagram detailing the geometry involved in the simple absorption model, which was used to convert the filtered absorption data into number distributions for the **FS-Hex** and **FS-TEG** water/methanol/TEA dispersions. The crux of the model revolves around estimating how much of a particle of diameter ( $d$ ) is actively absorbing during UV-vis measurements given the “420 nm 99% absorption depths” (referred to hereon in as just the “absorption depth”) calculated from the data in **Figure S-20** and **Figure S-24**. The decision to use the depth at which 99% of photons are absorbed as a cut-off was made to allow the problem to be solved without use of an integral.

This model is only intended to be a simple approximation in an attempt to highlight the substantial differences in the particle size distributions in the **FS-Hex** and **FS-TEG** dispersions, and thus includes a number of assumptions. Most importantly, the model assumes that there are only four particle sizes in the distribution, and that each filtration band from experiment can be represented by particles which are at the upper limit of that band (*i.e.* particles of 0.20, 0.45, 1.0 and 1.5  $\mu\text{m}$ , as described in the main text. The model also assumes that all particles in the dispersions are fully exposed to the UV-vis probe light at all times, with no obscuration or scattering from other particles. This is reasonable if the concentration in the measured samples is low enough; however, a minimum concentration was required to see appreciable absorption which most likely puts the measured samples a little beyond this limit. In order to reduce the problem to one of geometry only, the model also assumes that,

due to the rotational symmetry of the spherical particles and the speed of exciton generation and decay, all parts of the particle which are within the absorption depth in the direction of the probe beam are fully absorbing at all times. Other assumptions include the lack of internal scattering within the particle, the neglect of differences in polymer density within each particle, the neglect of differences in polymer density between films and particles, the modelling of particles as hard spheres with well-defined boundaries and the neglect of refractive or interference effects.

From the data in **Figure S-20** and **Figure S-24**, the absorption depths ( $A$ ) of **FS-TEG** and **FS-Hex** were estimated to be 189 nm and 282 nm respectively. The green shaded area in **Figure S-25** denotes the absorbing volume for particles in which  $d > A$ . For particles with  $d < A$ , the entire particle is assumed to be absorbing. This volume is calculated as follows: a second sphere is translated by a distance equal to the absorption depth in the direction of the probe beam. From symmetry and the knowledge of  $A$  and  $d$ , the height of the spherical cap height ( $h$ ) can be calculated. The volume of the spherical cap is then calculated using the formula:

$$V = \frac{1}{3}\pi h^2(3R - h)$$

The volume of the particle which is not green in the diagram (i.e. is not absorbing) is, by symmetry, twice the above volume. With the physical volume of the particle known from its diameter, the green absorbing volume can then be calculated by subtraction.

For both polymers, the absorbing volume was then calculated for particles of the four diameters. The “number of particles” of each diameter which existed in each sample was then estimated by dividing the 420 nm absorbance of each sample by this absorbing volume. The “number of particles” are only relative and can therefore only be used as a measure of the distribution of sizes.

**Molecular Dynamics Simulations.** Molecular dynamics simulations were performed using the same methodology as our previous work,<sup>13</sup> namely OPLS forcefields were used for the solvents and an OPLS-based forcefield was used for polymers. The polymer forcefield is based on the forcefields used in our previous work for the polymers **FSM1** and **P7** but replaces the bridging groups with the sidechains. The sidechain parameters are shown in Table. Simulations used short oligomers with an

equivalent length of six fluorene units (3-mers of **FS** polymers and 4-mers for **FP** polymers) as a model for the polymers. Oligomers were simulated in a 1:1 water/TEA mixture as well as the reaction medium, 1:1:1 of water/methanol/TEA. Radial distribution functions (RDFs) were calculated in order to calculate the volume occupied by each solvent as a function of distance from the oligomer backbone.

**Hydrogen evolution experiments.** Water for the hydrogen evolution experiments was purified using an ELGA LabWater system with a Purelab Option S filtration and ion exchange column without further pH level adjustment. For powder samples, a quartz flask was charged with the polymer powder (25 mg), water, TEA, methanol (1:1:1 mixture, 25 mL) and sealed with a septum. The resultant suspensions were ultrasonicated until the photocatalyst was dispersed before degassing by N<sub>2</sub> bubbling for 30 minutes. For film samples, glass substrates obtained from G & N Laboratory were first prepared for polymer deposition. OTS-functionalized slides were prepared using a literature method<sup>15</sup> while roughened glass substrates were roughened to opacity using sandpaper before cleaning by ultrasonication with water, methanol acetone and drying. In all cases, polymers were coated on these substrates by spin-coating solutions of chloroform (300  $\mu$ L) of specified concentration at 3000 rpm for 60 s before annealing at 80 °C for two hours. A quartz cuvette was charged with water containing 5 vol. % triethylamine (8 mL) before immersion of the polymer-coated slide, sealing with a septum and degassing for 15 minutes. All reaction mixtures were then illuminated with a 300 W Newport Xe light source (Model: 6258, Ozone free) for the time specified using appropriate filters. NIR light was absorbed by circulating water through a fused silica window. Alternatively, an Oriel LSH-7320 ABA LED-based Solar Simulator with an AM 1.5 G output of 1 sun was used. Gas samples were taken with a gas-tight syringe and run on a Bruker 450-GC gas chromatograph equipped with a Molecular Sieve 13X 60-80 mesh 1.5 m  $\times$  1/8"  $\times$  2 mm ss column at 50 °C with an argon flow of 40.0 mL min<sup>-1</sup>. Hydrogen was detected with a thermal conductivity detector referencing against standard gas with a known concentration of hydrogen. Hydrogen dissolved in the reaction mixture was not measured and the pressure increase generated by the evolved hydrogen was neglected in the calculations. The rates were determined from a linear regression fit once a consistent rate of increase of hydrogen evolution was observed and the error is given as the standard deviation of the amount of hydrogen evolved over this time. No hydrogen evolution was observed for a mixture of water/methanol/triethylamine under  $\lambda$



> 295 nm illumination in absence of a photocatalyst.

**External quantum efficiency measurements:** FS-TEG (12 mg) was dispersed in water, triethylamine, and methanol (1:1:1 vol. mixture, 8 mL) by ultrasonication, degassed for 30 minutes with nitrogen, and irradiated with a  $\lambda = 420$  nm LED controlled by an IsoTech IPS303DD power supply. An area of 8 cm<sup>2</sup> was illuminated and the light intensity was measured with a ThorLabs S120VC photodiode power sensor controlled by a ThorLabs PM100D Power and Energy Meter Console to be 2.89 mW cm<sup>-2</sup>. The external quantum efficiencies were estimated using the equation below:

$$EQE = 2 \text{ \AA} \frac{\text{moles of hydrogen evolved}}{\text{moles of incident photons}} \text{ \AA} 100\%$$

**Scaled-up photoreactor preparation and hydrogen evolution experiments.** The photoreactor comprised a chamber containing polymer-coated glass wool suspended in 5 vol.% TEA in water which was connected by tubing to an upturned measuring cylinder filled with water to measure the volume of evolved hydrogen. Karl Hecht glass wool (45 g, obtained from LabUnlimited, textile glass fibers with a nominal diameter of 8 - 50 $\mu$ m) was coated with **FS-TEG** (165 mg) by evaporation from chloroform. The polymer-coated glass fibers were then submerged in 950 mL of 5 vol. % TEA in the photoreactor chamber before the set-up was sealed. The volume of evolved hydrogen was measured hourly on a partially cloudy August afternoon in Liverpool, U.K.

**General procedure for the synthesis of polymers via Suzuki-Miyaura-type polycondensation.** A flask was charged with the monomers, toluene, Starks' catalyst, and an aqueous solution of Na<sub>2</sub>CO<sub>3</sub>. The mixture was degassed by bubbling with N<sub>2</sub> for 30 minutes, before [Pd(PPh<sub>3</sub>)<sub>4</sub>] was added, and heated. The mixtures were evaporated to dryness and washed with water. The crude polymer was then further purified by Soxhlet extraction with methanol, acetone, and ethyl acetate. The high molecular weight fraction of the polymer was recovered by Soxhlet extraction with chloroform. The chloroform was removed and the polymer redissolved in a minimal amount of chloroform, precipitated into a large excess of

methanol, filtered off and dried under reduced pressure. Note: For all polymers the yields were calculated ignoring the presence of end functional groups whose nature is unclear.

**Synthesis of FP-Hex:** 1,4-Benzenediboronic acid bis(pinacol) ester (660 mg, 2.0 mmol), 2,7-dibromo-9,9-di-*n*-hexyl-9*H*-fluorene (985 mg, 2.0 mmol), toluene (35 mL), Na<sub>2</sub>CO<sub>3</sub> (15 mL, 2 M), Starks' catalyst (2 drops), and [Pd(PPh<sub>3</sub>)<sub>4</sub>] (35 mg) were used in this reaction. After 2 days at 110 °C the reaction was worked up as described above giving the product as a grey solid in 47% yield (0.384 g). Anal. Calcd for **FP-Hex** (C<sub>31</sub>H<sub>36</sub>)<sub>*n*</sub>: C, 91.12; H, 8.88%. Found: C, 89.27; H, 8.75; Pd, 0.48%. <sup>1</sup>H NMR (400 MHz, CDCl<sub>3</sub>) δ: 7.93-7.53 (10 H, m), 2.09 (4 H, s, br), 1.11 (12 H, m), 0.79 (10 H, m).

**Synthesis of FP-EtHex:** 1,4-Benzenediboronic acid bis(pinacol) ester (660 mg, 2.0 mmol), 2,7-dibromo-9,9-bis(2-ethylhexyl)fluorene (1100 mg, 2.0 mmol), toluene (35 mL), Na<sub>2</sub>CO<sub>3</sub> (15 mL, 2 M), Starks' catalyst (2 drops), and [Pd(PPh<sub>3</sub>)<sub>4</sub>] (35 mg) were used in this reaction. After 2 days at 110 °C the reaction was worked up as described above giving the product as a grey solid in 90% yield (837 mg). Anal. Calcd for **FP-EtHex** (C<sub>35</sub>H<sub>44</sub>)<sub>*n*</sub>: C, 90.46; H, 9.54%. Found: C, 89.16; H, 9.41; Pd, 0.38%. <sup>1</sup>H NMR (400 MHz, CDCl<sub>3</sub>) δ: 7.92-7.60 (10 H, m), 2.12 (4 H, s, br), 0.89 (18 H, m), 0.71-0.62 (6 H, m), 0.62-0.53 (6 H, m).

**Synthesis of FP-Oct:** 1,4-Benzenediboronic acid bis(pinacol) ester (660 mg, 2.0 mmol), 2,7-dibromo-9,9-di-*n*-octyl-9*H*-fluorene (1100 mg, 2.0 mmol), toluene (35 mL), Na<sub>2</sub>CO<sub>3</sub> (15 mL, 2 M), Starks' catalyst (2 drops), and [Pd(PPh<sub>3</sub>)<sub>4</sub>] (35 mg) were used in this reaction. After 2 days at 110 °C the reaction was worked up as described above giving the product as a grey solid in 72% yield (0.669 g). Anal. Calcd for **FP-Oct** (C<sub>35</sub>H<sub>44</sub>)<sub>*n*</sub>: C, 90.46; H, 9.54%. Found: C, 89.15; H, 9.44; Pd, 0.44%. <sup>1</sup>H NMR (400 MHz, CDCl<sub>3</sub>) δ: 7.7-7.91 (6 H, m), 7.61-7.73 (4 H, m), 2.09 (4 H, s, br), 1.01-1.26 (20 H, m), 0.7-0.85 (10 H, m).

**Synthesis of FP-Dodec:** 1,4-Dibromobenzene (472 mg, 2.0 mmol), 9,9-Di-*n*-dodecyl-9*H*-fluorene-2,7-diyl-diboronic acid (1.18 g, 2.0 mmol), toluene (35 mL), Na<sub>2</sub>CO<sub>3</sub> (15 mL, 2 M), Starks' catalyst (2 drops), and [Pd(PPh<sub>3</sub>)<sub>4</sub>] (35 mg) were used in this reaction. After 2 days at 110 °C the reaction was worked up as described above giving the product as a grey solid in 57% yield (0.642 g). Anal. Calcd for **FP-Dodec** (C<sub>43</sub>H<sub>60</sub>)<sub>*n*</sub>: C, 89.52; H, 10.48%. Found: C, 87.43; H, 10.28; Pd, 0.43%. <sup>1</sup>H NMR (400MHz, CDCl<sub>3</sub>) δ: 7.66-7.86 (6 H, m), 7.60-7.72 (4 H, m), 2.08 (4 H, s, br), 1.03-1.34 (40 H, m), 0.85 (6 H, t, *J* = 5.0 Hz).

**Synthesis of FP-TEG:** 2,7-Dibromo-9,9-bis[2-[2-(2-methoxyethoxy)ethoxy]ethyl]-9*H*-fluorene (0.650 g, 1.1 mmol), 1,4-benzenediboronic acid bis(pinacol) ester (0.355 g, 1.1

mmol), [Pd(PPh<sub>3</sub>)<sub>4</sub>] (26.5 mg, 0.02 mmol), toluene (20 mL) and aqueous Na<sub>2</sub>CO<sub>3</sub> (2.0 M, 7 mL) were used in this reaction. After work-up and Soxhlet extraction with chloroform, the soluble product was obtained as a grey-brown powder (0.096 g, 17%). Anal. Calcd for **FP-TEG** (C<sub>33</sub>H<sub>40</sub>O<sub>6</sub>)<sub>n</sub>: C, 74.41; H, 7.57%. Found: C, 71.78; H, 7.29; Pd, 0.43%. <sup>1</sup>H NMR (400 MHz, CDCl<sub>3</sub>) δ: 7.66-7.88 (10 H, m) 3.37-3.56 (16 H, m), 3.31 (10 H, t, *J* = 9.0 Hz), 2.93 (4 H, s, br), 2.54 (4 H, s, br).

**Synthesis of FS-Hex:** 9,9-Di-*n*-hexylfluorene-2,7-diboronic acid (844 mg, 2.0 mmol), 3,7-dibromodibenzo[*b,d*]thiophene sulfone (748 mg, 2.0 mmol), toluene (35 mL), Na<sub>2</sub>CO<sub>3</sub> (15 mL, 2 M), Starks' catalyst (2 drops), and [Pd(PPh<sub>3</sub>)<sub>4</sub>] (35 mg) were used in this reaction. After 2 days at 110 °C the reaction was worked up as described above giving the product as a green-yellow solid in 50% yield (550 mg). Anal. Calcd for **FS-Hex** (C<sub>37</sub>H<sub>38</sub>O<sub>2</sub>S)<sub>n</sub>: C, 81.28; H, 7.01; S, 5.86%. Found: C, 79.14; H, 6.86; S, 5.76; Pd, 0.04%. <sup>1</sup>H NMR (400MHz, CDCl<sub>3</sub>) δ: 8.14 (2 H, s), 7.81-8.00 (6 H, m), 7.63-7.73 (4 H, m), 1.93-2.25 (4 H, m), 1.01-1.20 (12 H, m), 0.60-0.83 (10 H, m). Note: An insoluble fraction was also obtained in 40% yield (439 mg).

**Synthesis of FS-EtHex:** 9,9-Di(2-ethylhexyl)fluorene-2,7-diboronic acid bis(1,3-propanediol) ester (2 mL, 0.5 M solution in toluene), 3,7-dibromodibenzo[*b,d*]thiophene sulfone (374 mg, 2.0 mmol), toluene (17.5 mL), Na<sub>2</sub>CO<sub>3</sub> (7.5 mL, 2 M), Starks' catalyst (2 drops), and [Pd(PPh<sub>3</sub>)<sub>4</sub>] (17.5 mg) were used in this reaction. After 2 days at 110 °C the reaction was worked up as described above giving the product as a green solid in 63% yield (382 mg). Anal. Calcd for **FS-EtHex** (C<sub>41</sub>H<sub>46</sub>O<sub>2</sub>S)<sub>n</sub>: C, 81.68; H, 7.69; S, 5.32%. Found: C, 81.18; H, 7.79; S, 5.12; Pd, 0.32%. <sup>1</sup>H NMR (400 MHz, CDCl<sub>3</sub>) δ: 8.14 (2 H, s), 7.81-8.00 (6 H, m), 7.63-7.73 (4 H, m), 2.12 (4 H, s, br), 0.73-1.01 (18 H, m), 0.50-0.72 (12 H, m).

**Synthesis of FS-Oct:** 2,2'-(9,9-Di-*n*-octyl-9*H*-fluorene-2,7-diyl-bis(4,4,5,5-tetramethyl-1,3,2-dioxaborolane) 643 mg, 1.0 mmol), 3,7-dibromodibenzo[*b,d*]thiophene sulfone (374 mg, 1.0 mmol), toluene (17.5 mL), Na<sub>2</sub>CO<sub>3</sub> (7.5 mL, 2 M), Starks' catalyst (2 drops), and [Pd(PPh<sub>3</sub>)<sub>4</sub>] (17.5 mg) were used in this reaction. After 2 days at 110 °C the reaction was worked up as described above giving the product as a green solid in 37% yield (248 mg). Anal. Calcd for **FS-Oct** (C<sub>41</sub>H<sub>46</sub>O<sub>2</sub>S)<sub>n</sub>: C, 81.68; H, 7.69; S, 5.32%. Found: C, 81.30; H, 7.70; S, 5.31; Pd, 0.02%. <sup>1</sup>H NMR (400 MHz, CDCl<sub>3</sub>) δ: 8.19 (2 H, s), 7.83-8.04 (6 H, m), 7.61-7.72 (4 H, m), 2.12 (4 H, s, br), 1.01-1.30 (20 H, m), 0.7-0.85 (10 H, m).

**Synthesis of FS-Dodec:** 9,9-Di-*n*-dodecyl-9*H*-fluorene-2,7-diyl-diboronic acid (591 mg, 1.0 mmol), 3,7-dibromodibenzo[*b,d*]thiophene sulfone (374 mg, 1.0 mmol), toluene (17.5 mL), Na<sub>2</sub>CO<sub>3</sub> (7.5 mL, 2 M), Starks' catalyst (2 drops), and [Pd(PPh<sub>3</sub>)<sub>4</sub>] (17.5 mg) were used in this reaction. After 2 days at 110 °C the reaction was worked up as described above giving the product as a dark green solid in 79% yield (561 mg). Anal. Calcd for **FS-Dodec** (C<sub>49</sub>H<sub>62</sub>O<sub>2</sub>S)<sub>*n*</sub>: C, 81.91; H, 8.74; S, 4.48%. Found: C, 81.97; H, 8.88; S, 4.29; Pd, 0.07%. <sup>1</sup>H NMR (400MHz, CDCl<sub>3</sub>) δ: 8.19 (2 H, s), 7.83-8.03 (6 H, m), 7.61-7.72 (4 H, m), 2.12 (4 H, s, br), 1.03-1.32 (40 H, m), 0.84 (6 H, t, *J* = 6.0 Hz).

**Synthesis of FS-TEG:** 2,7-Dibromo-9,9-bis[2-[2-(2-methoxyethoxy)ethoxy]ethyl]-9*H*-fluorene (0.6164 g, 1.0 mmol), dibenzo[*b,d*]thiophene sulfone diboronic acid bis(pinacol) ester (0.4682 g, 1.0 mmol), [Pd(PPh<sub>3</sub>)<sub>4</sub>] (17.5 mg, 0.02 mmol), toluene (17.5 mL) and aqueous Na<sub>2</sub>CO<sub>3</sub> (2.0 M, 7.5 mL) were used in this reaction. After work-up and Soxhlet extraction with chloroform, the soluble product was obtained as a dark green powder (0.483 g, 74%). Anal. Calcd for **FS-TEG** (C<sub>39</sub>H<sub>42</sub>O<sub>8</sub>S)<sub>*n*</sub>: C, 69.83; H, 6.31; S, 4.78%; Found: C, 68.47; H, 6.19; S, 4.64; Pd, 0.30%. <sup>1</sup>H NMR (400MHz, CDCl<sub>3</sub>) δ: 8.18 (2 H, s), 7.81-8.06 (6 H, m), 7.64-7.79 (4 H, m), 3.11-3.53 (26 H, overlapped peaks), 2.89 (4 H, s, br), 2.55 (4 H, s, br).

## 1. $^1\text{H}$ NMR Spectroscopy

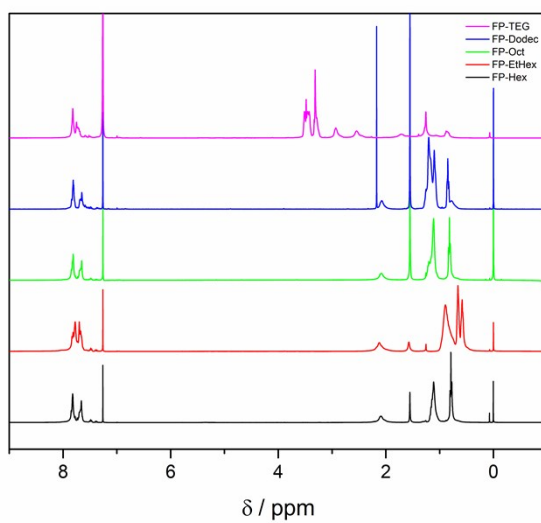


**Figure S-1.**  $^1\text{H}$  NMR spectra of the **FP** series in  $\text{CDCl}_3$ . Peaks of residual impurities correspond to chloroform (7.26 ppm) and water (1.56 ppm).

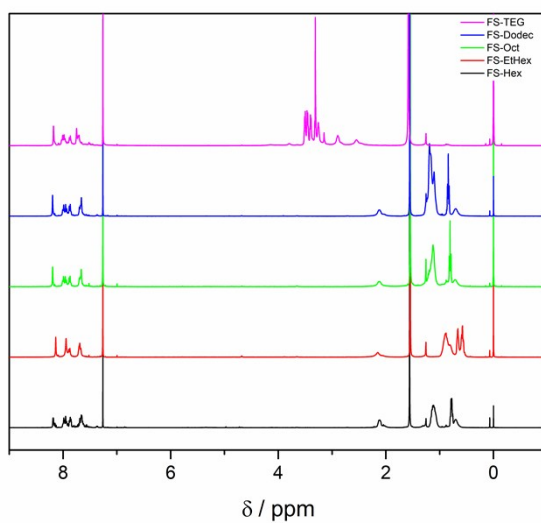


**Figure S-2.**  $^1\text{H}$  NMR spectra of the **FS** series in  $\text{CDCl}_3$ . Peaks of residual impurities correspond to chloroform (7.26 ppm) and water (1.56 ppm).

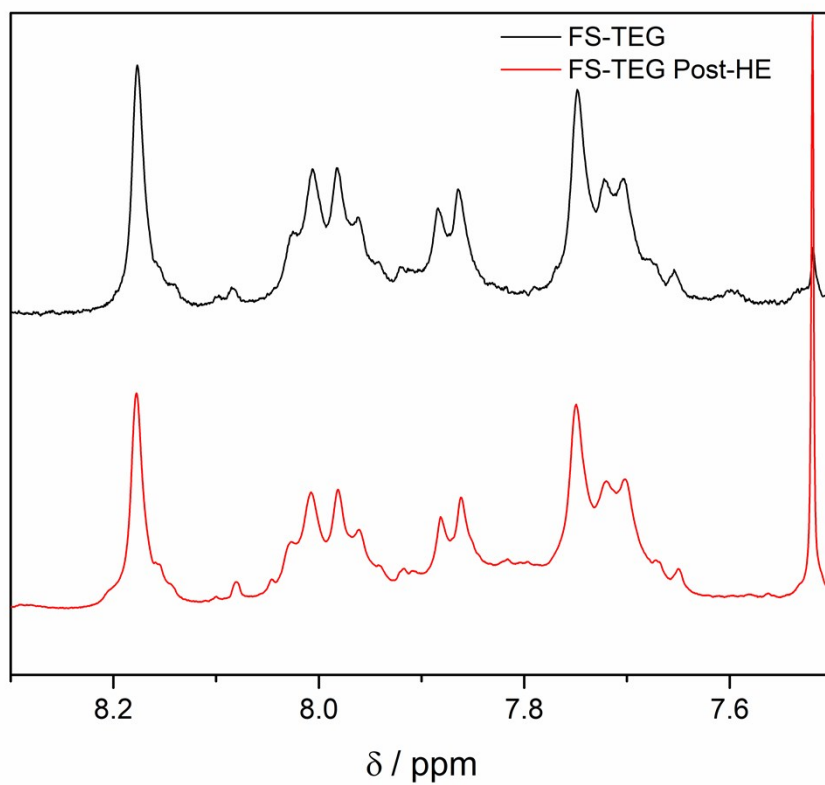


**Figure S-3.** <sup>1</sup>H NMR spectra of **FS-TEG** in CDCl<sub>3</sub> before and after hydrogen evolution experiments (Post-HE = after 5 hours in water/methanol/TEA,  $\lambda > 420$  nm, 300 W Xe light source). Peaks of residual impurities correspond to chloroform (7.26 ppm), water (1.56 ppm)

## 2. Gel Permeation Chromatography

**Table S-1.** GPC data for all chloroform-soluble polymer fractions.

<b>Polymer</b>	$M_n^a$ / g mol <sup>-1</sup>	$M_w^a$ / g mol <sup>-1</sup>	<b><math>\bar{D}</math></b>
FP-Hex	18,200	43,200	4.40
FP-EtHex	14,600	39,000	2.67
FP-Oct	16,300	57,900	3.55
FP-Dodec	6600	12,900	1.95
FP-TEG	8200	12,300	1.51
FS-Hex	3800	8200	2.16
FS-EtHex	19,000	36,900	1.94
FS-Oct	18,900	31,900	1.69
FS-Dodec	14,900	25,400	1.70
FS-TEG	8700	11,500	1.35

[a] Obtained from gel permeation chromatography in chloroform calibrated against polystyrene standards.

### 3. Powder X-Ray Diffraction

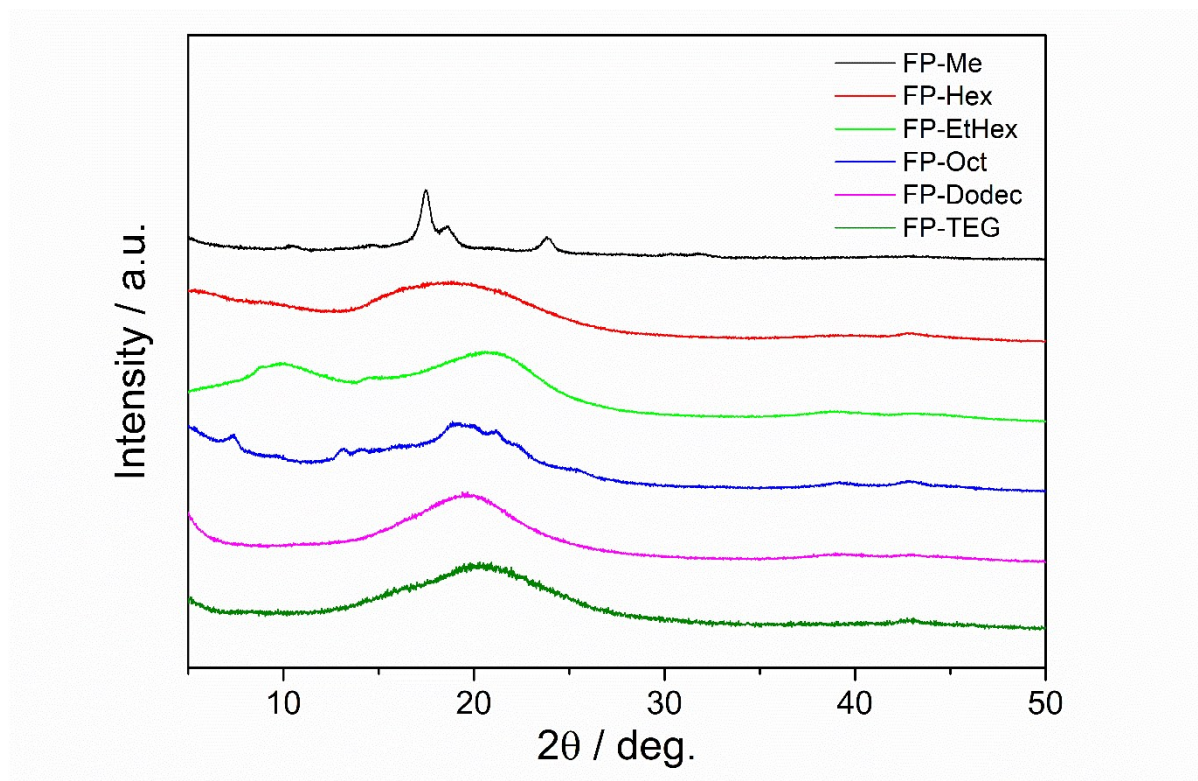


Figure S-4. PXRd patterns of FP-Me, FP-Hex, FP-EtHex, FP-Oct, FP-Dodec and FP-TEG.

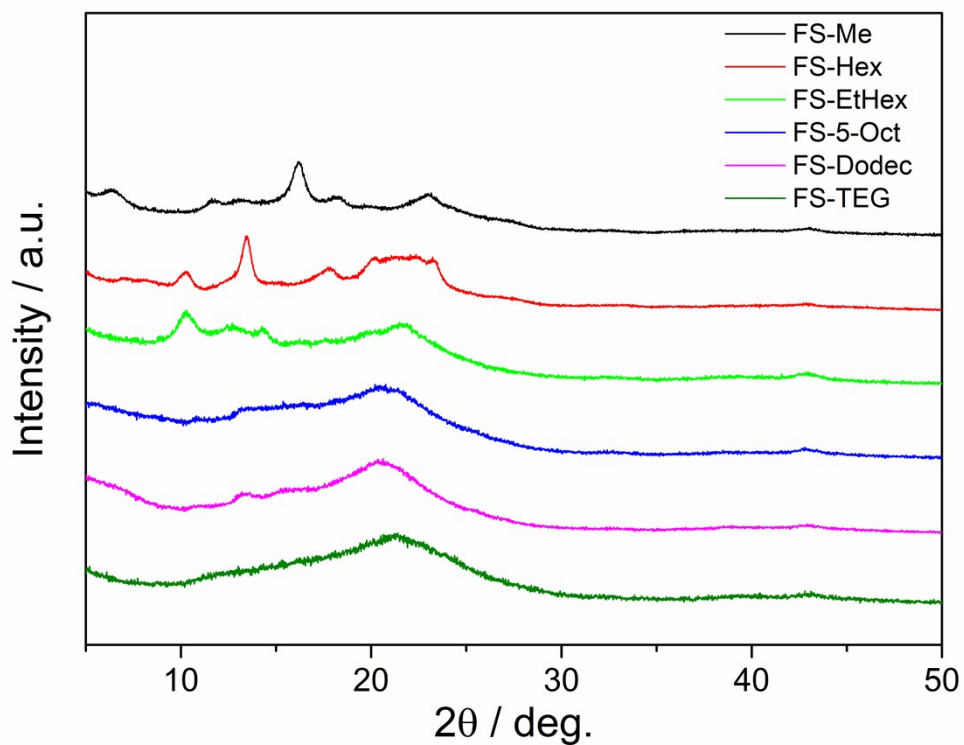
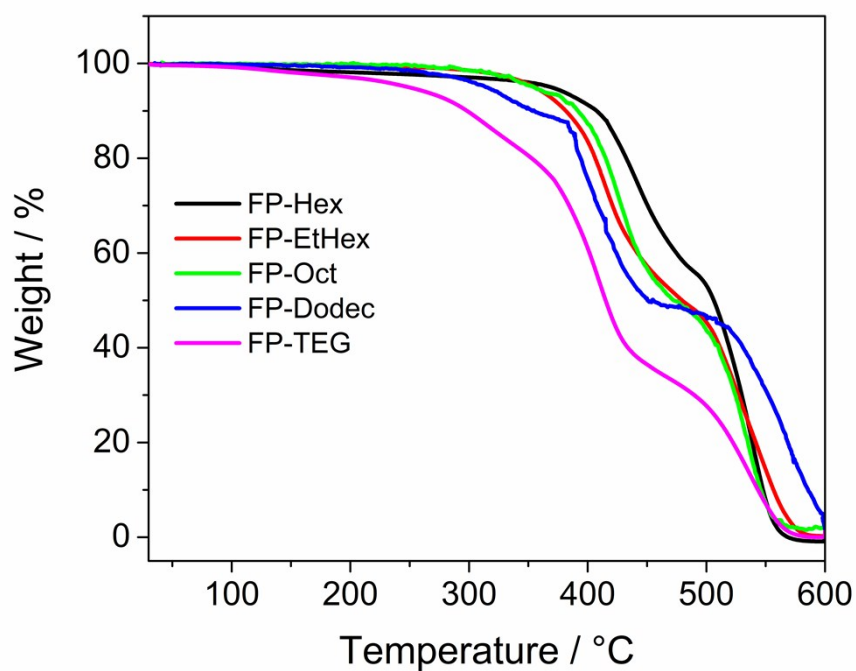


Figure S-5. PXRd pattern of FS-Me, FS-Hex, FS-EtHex, FS-Oct, FS-Dodec and FS-TEG.



#### 4. Thermogravimetric Analysis



**Figure S-6.** Thermogravimetric analysis of FP-Hex, FP-EtHex, FP-Oct, FP-Dodec and FP-TEG in air at a heating rate of 10 °C min<sup>-1</sup>.

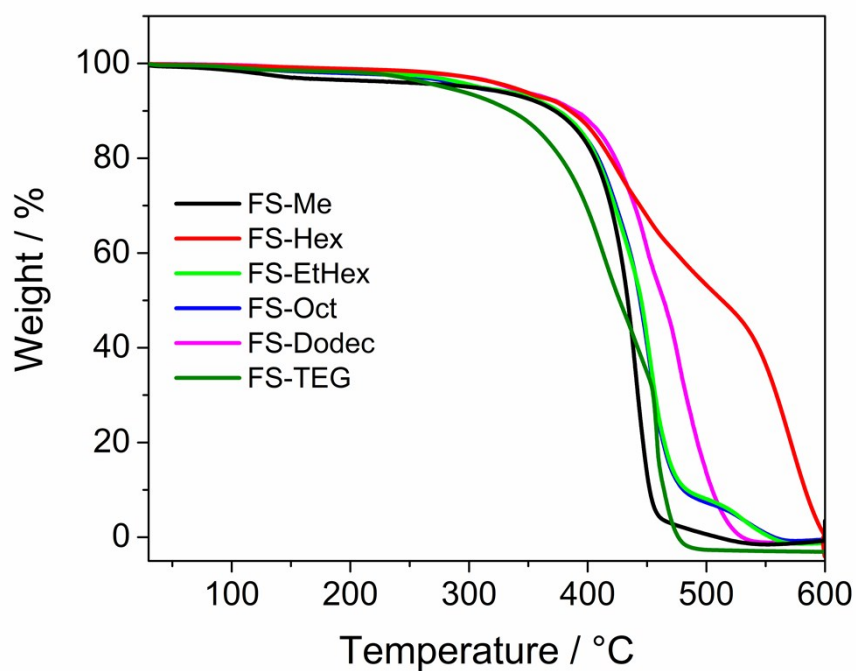


**Figure S-7.** Thermogravimetric analysis of FS-Me, FS-Hex, FS-EtHex, FS-Oct, FS-Dodec and FS-TEG in air at a heating rate of 10 °C min<sup>-1</sup>.

## 5. UV-Vis and Photoluminescence Spectra

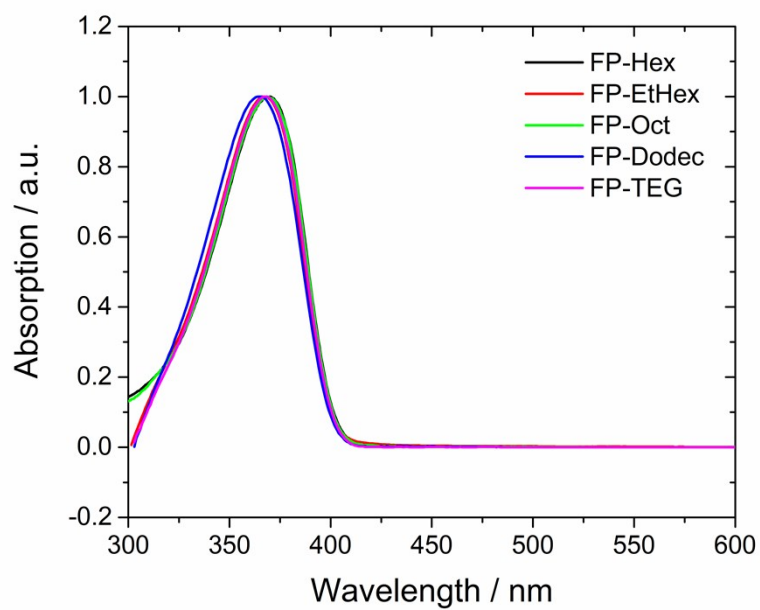


**Figure S-8.** UV-Vis absorption spectra of the **FP** series dissolved in chloroform.

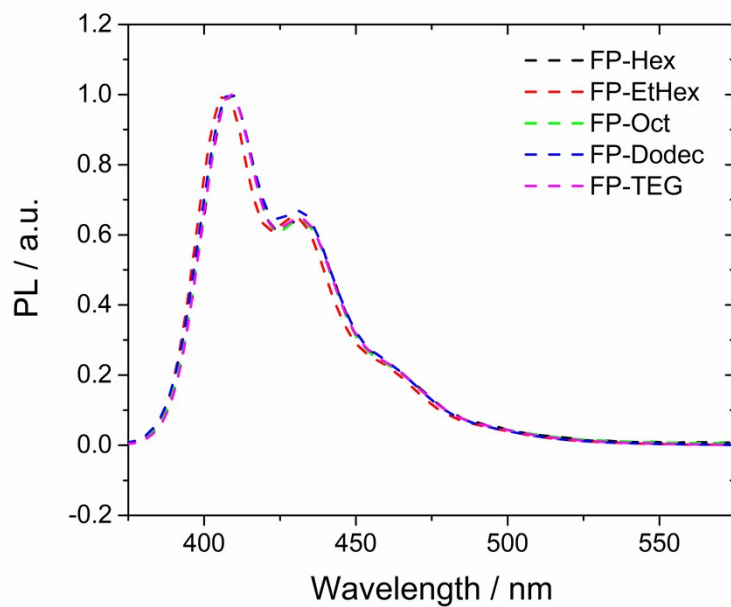


**Figure S-9.** Photoluminescence spectra of the **FP** series dissolved in chloroform.

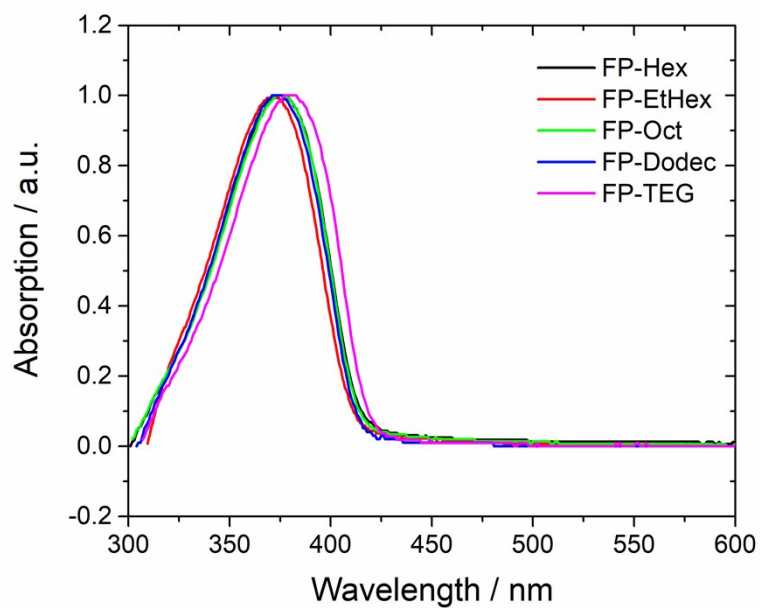


**Figure S-10.** UV-Vis absorption spectra of thin films of the **FP** series spin-coated on glass substrates from chloroform.

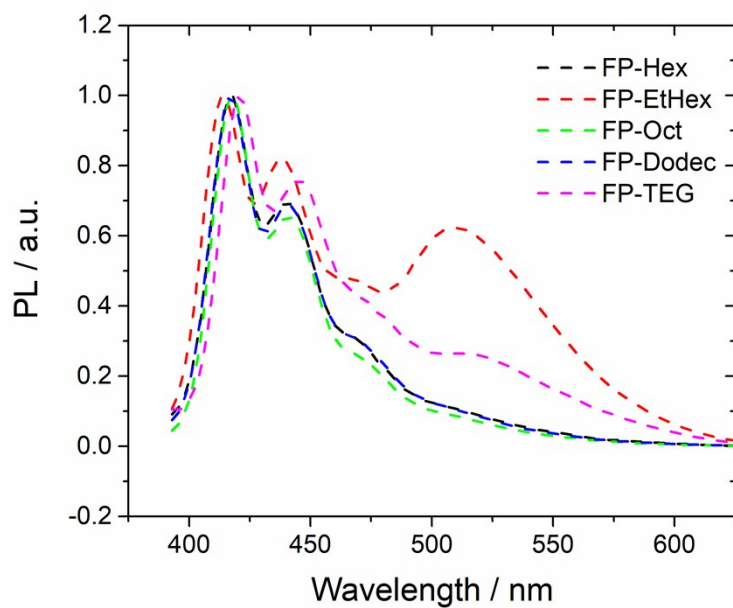


**Figure S-11.** Photoluminescence spectra of thin films of the **FP** series spin-coated on glass substrates from chloroform.

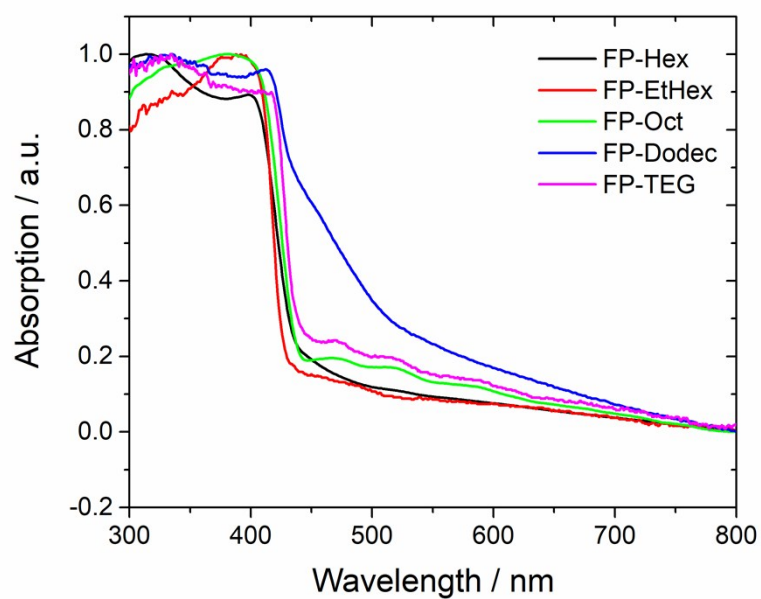


**Figure S-12.** UV-Vis absorption spectra of the **FP** series in powdered form. Onset of absorbance in powders appear slightly red-shifted compared to the same materials as thin films, due to the much greater optical depth of the powders.

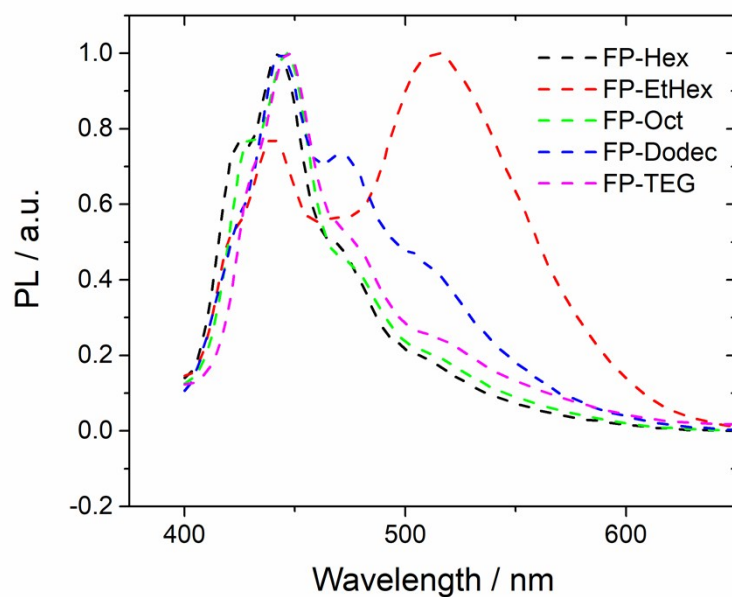


**Figure S-13.** Photoluminescence spectra of the **FP** series in powdered form

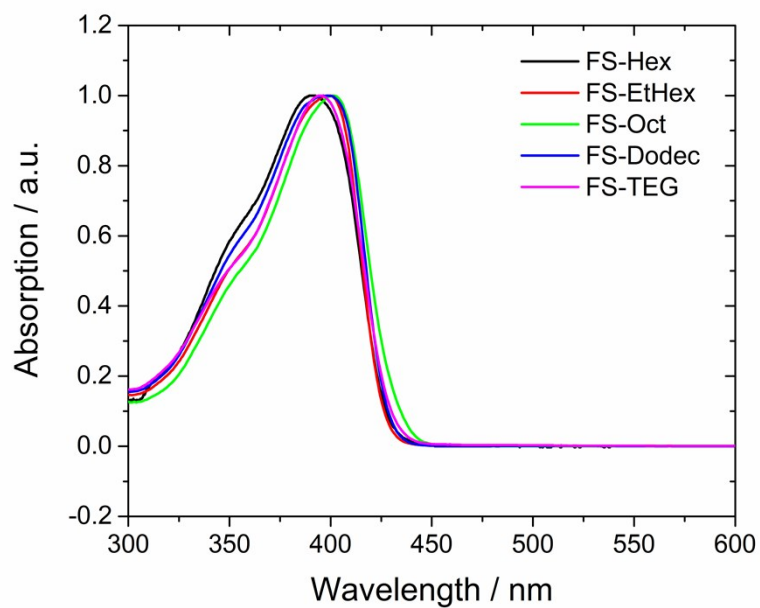


**Figure S-14.** UV-Vis absorption spectra of the **FS** series dissolved in chloroform.

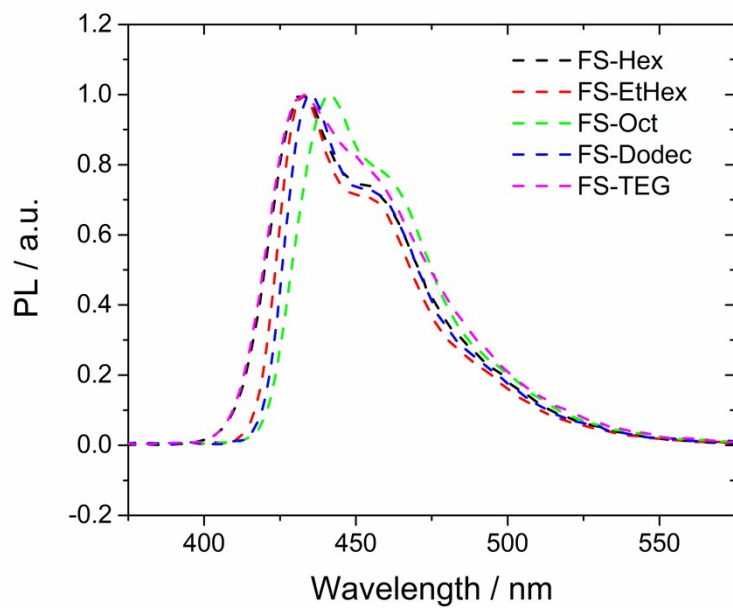


**Figure S-15.** Photoluminescence spectra of the **FS** series dissolved in chloroform.

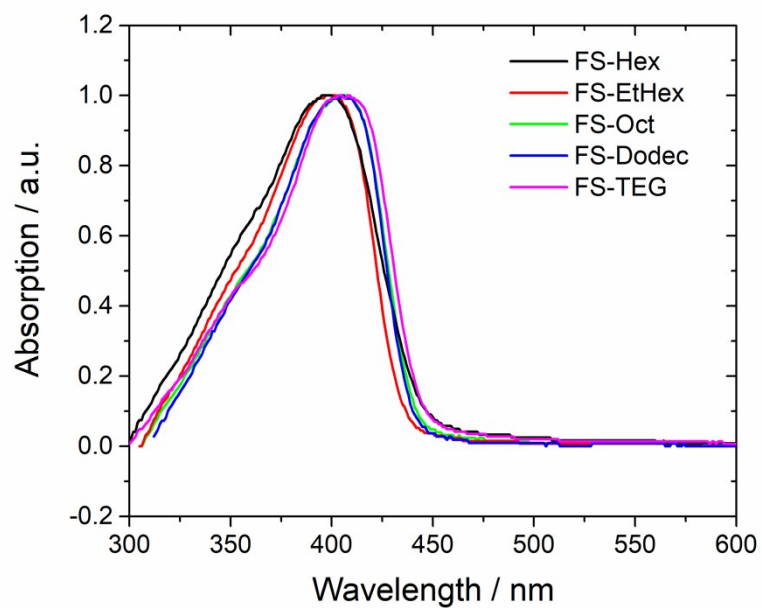


**Figure S-16.** UV-Vis absorption spectra of thin films of the **FS** series spin-coated on glass substrates from chloroform.

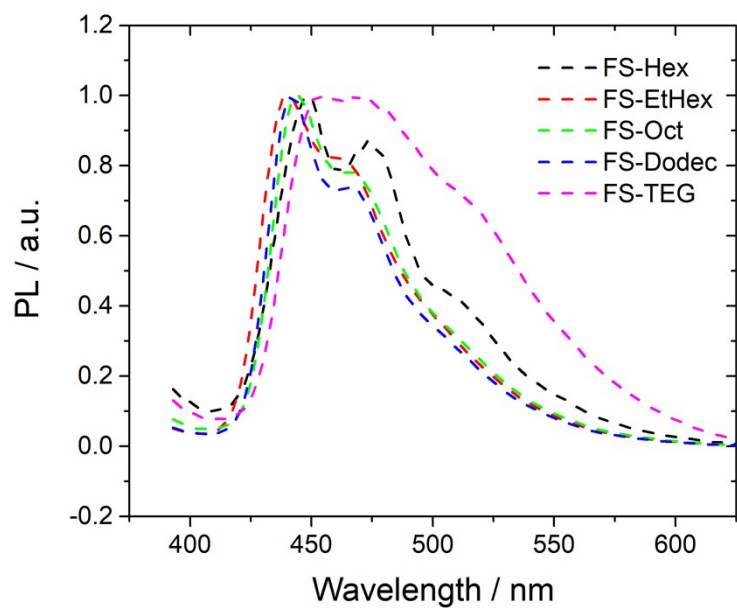


**Figure S-17.** Photoluminescence spectra of thin films of the **FS** series spin-coated on glass substrates from chloroform

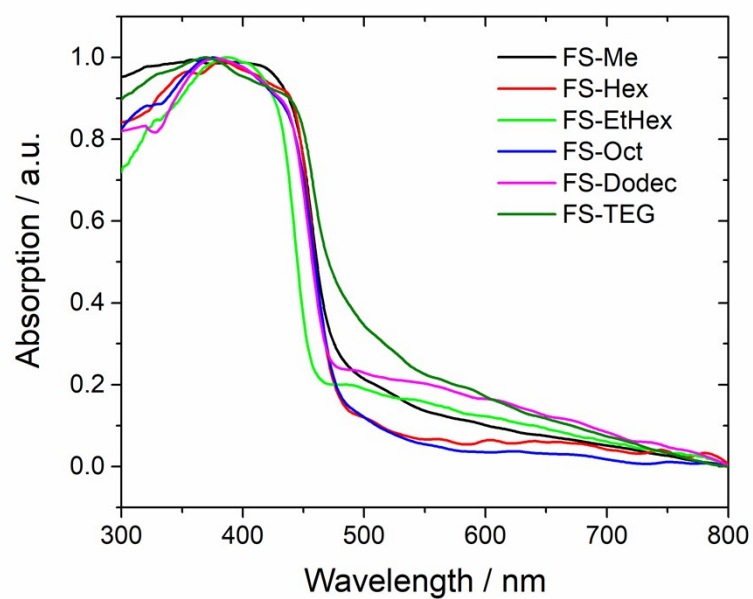


**Figure S-18.** UV-Vis absorption spectra of the **FS** series in powdered form. Onset of absorbance in powders appear slightly red-shifted compared to the same materials as thin films, due to the much greater optical depth of the powders.

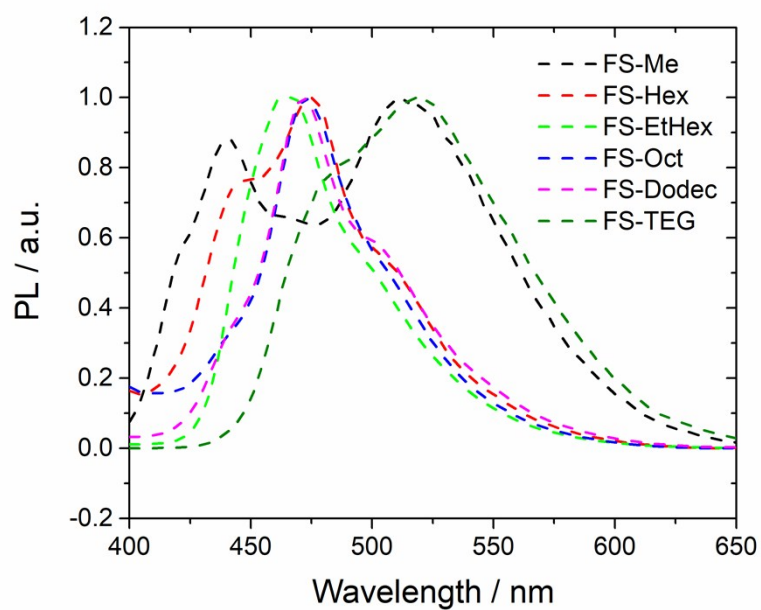


**Figure S-19.** Photoluminescence spectra of the **FS** series in powdered form

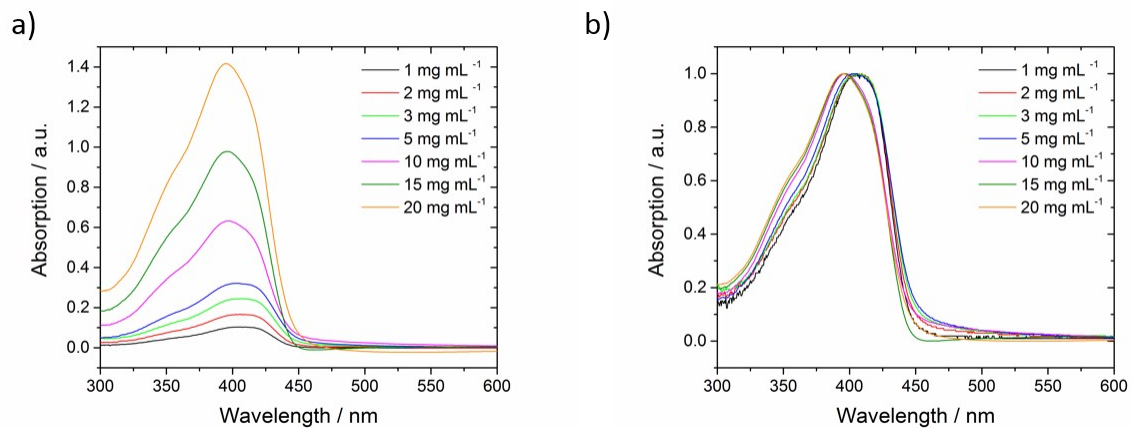


**Figure S-20.** UV-Vis absorption spectra of films of **FS-TEG** series spin-coated from solutions of chloroform of varying concentrations (300  $\mu$ L on  $26 \times 16$  mm OTS-functionalised glass slides). Spectra are **a)** not normalized and **b)** normalized.



## 6. (TD-)DFT Calculations

**Table S-2.** (TD-)B3LYP predicted optoelectronic properties of oligomers of **FP** and **FS**. Potentials are reported vs the standard hydrogen electrode (SHE, -4.44 V).

Series	Structure	$\hat{\mu}^{[a]}$	R	IP / V	EA / V	IP* / V	EA* / V	S0 $\rightarrow$ S1 / eV	f		
CFP		80.10	H	0.7301	-2.3760	-2.1386	0.5147	3.1579	4.1944		
			CH <sub>3</sub>	0.7425	-2.3637	-2.1358	0.5147	3.1552	4.1895		
		4.81	H	-	-	-	-	-	-	-	
			CH <sub>3</sub>	-	-	-	-	3.1509	4.1870		
		2.38	H	1.1383	-2.9362	-1.7727	-0.0253	3.2047	4.0184		
			CH <sub>3</sub>	1.1304	-2.9296	-1.7619	-0.0302	3.1499	4.1870		
		2.00	H	1.1967	-3.0121	-	-	-	-		
			CH <sub>3</sub>	1.1865	-2.9973	-	-	-	-		
		FS		80.10	H	0.9981	-1.9217	-1.7345	0.9013	2.9107	3.4655
					CH <sub>3</sub>	1.0064	-1.9010	-1.7679	0.8733	2.9135	3.2140
4.81	H			-	-	-	-	-	-		
	CH <sub>3</sub>			-	-	-	-	2.9486	3.2748		
2.38	H			1.4864	-2.4006	-1.2623	0.3481	2.9586	3.2835		
	CH <sub>3</sub>			1.4674	-2.3945	-1.3023	0.3752	2.9541	3.3130		
2.00	H			1.5515	-2.4629	-	-	-	-		
	CH <sub>3</sub>			1.5334	-2.4581	-	-	-	-		

[a] Dielectric constant used in COSMO implicit solvent model for Turbomole calculations.

## 7. Static Light Scattering

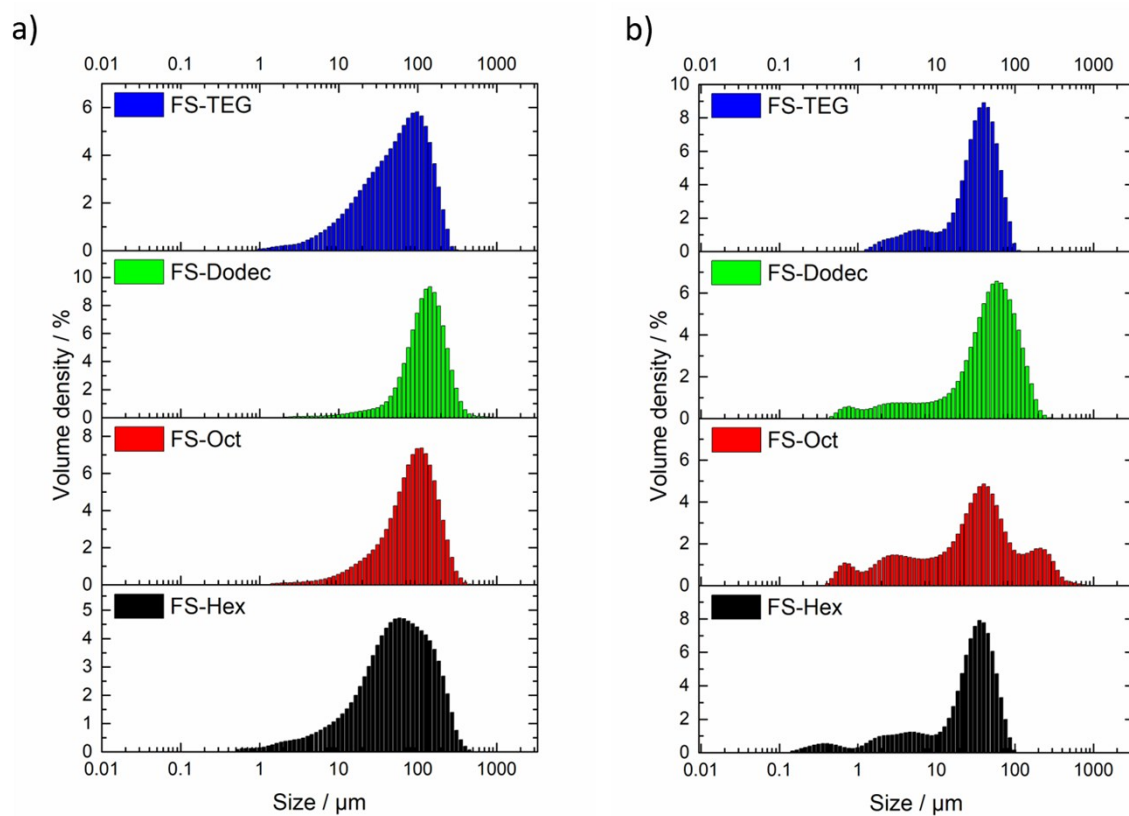


**Figure S-21.** Particle size distributions of **FS-Hex**, **FS-Oct**, **FS-Dodec** and **FS-TEG** obtained from static light scattering measurements in a) water and b) water/methanol/TEA (1:1:1).

**Table S-3.** Particle sizes by static light scattering.

<b>Medium</b>	<b>Polymer</b>	<b><math>D_x50^{[a]}</math></b> <b>/ <math>\mu\text{m}</math></b>	<b><math>D[4,3]^{[b]}</math></b> <b>/ <math>\mu\text{m}</math></b>	<b><math>D[3,2]^{[c]}</math></b> <b>/ <math>\mu\text{m}</math></b>
<b>Water</b>	FS-Hex	58.4	82.7	18.9
	FS-Oct	92.9	106	45.4
	FS-Dodec	135	149	79.5
	FS-TEG	61.8	75.3	25.7
<b>Water/MeOH/TEA</b>	FS-Hex	29.7	30.9	4.3
	FS-Oct	33.3	63.1	6
	FS-Dodec	51.4	59.6	10.6
	FS-TEG	35.8	37.3	16.2

[a] 50<sup>th</sup> Percentile of particle size volume distribution; [b] Volume mean diameter; [c] Surface area mean diameter (Sauter mean diameter).

## 8. Filtration Study

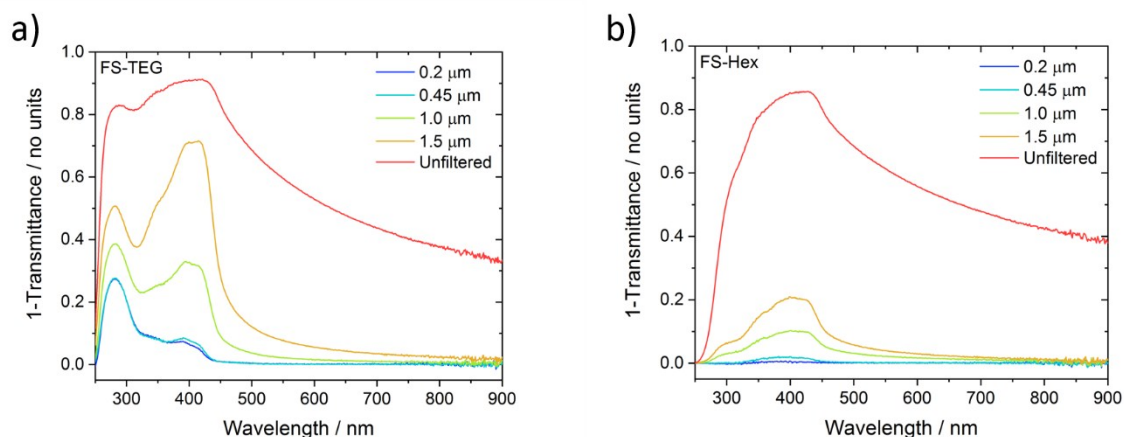


**Figure S-22.** 1-Transmittance data for (a) **FS-TEG** and (b) **FS-Hex** filtered samples in 1 mm quartz cuvettes. **FS-Hex** and **FS-TEG** were made up at  $1 \text{ mg ml}^{-1}$  in water/methanol/TEA, sonicated for 8 hours and then filtered with nylon filters of specified pore sizes.

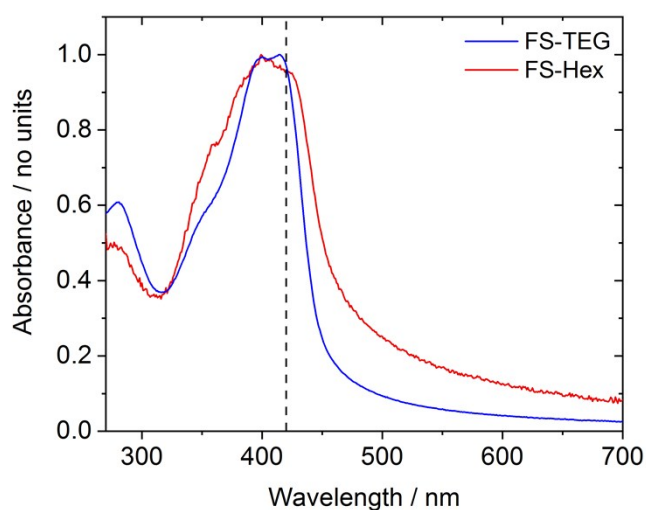


**Figure S-23.** Absorbance data seen in Figure 2 of the main text, normalised to highlight the difference in scattering tails. **FS-Hex** and **FS-TEG** were made up at  $1 \text{ mg ml}^{-1}$  in water/methanol/TEA, sonicated for 8 hours, filtered with nylon filters of specified pore sizes and measured in 1 mm quartz cuvettes.

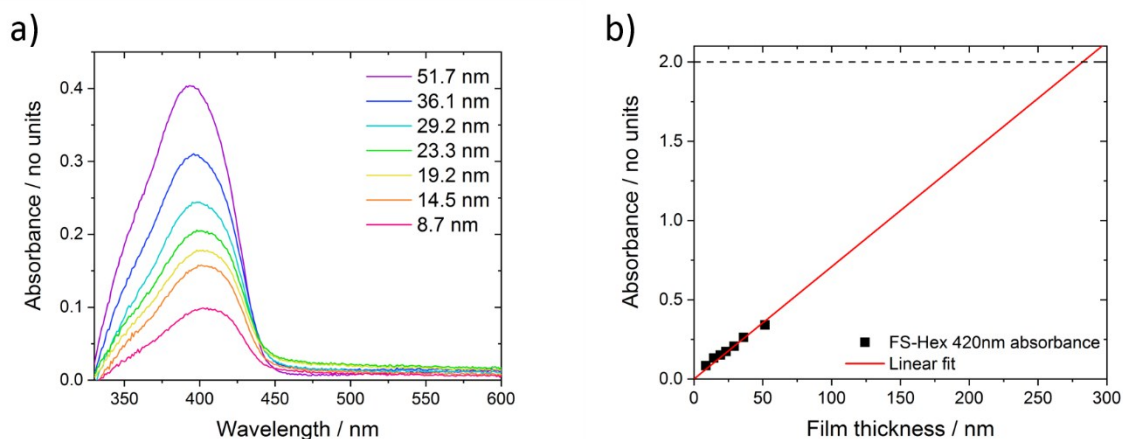


**Figure S-24.** Absorption-thickness calibration for **FS-Hex**. (a) Raw absorption data for films of different thickness, with thicknesses measured with a Dektak profilometer. (b) Absorption vs thickness plot, with extrapolated linear fit. 99% of photons are estimated to be absorbed within 282 nm (absorbance = 2).

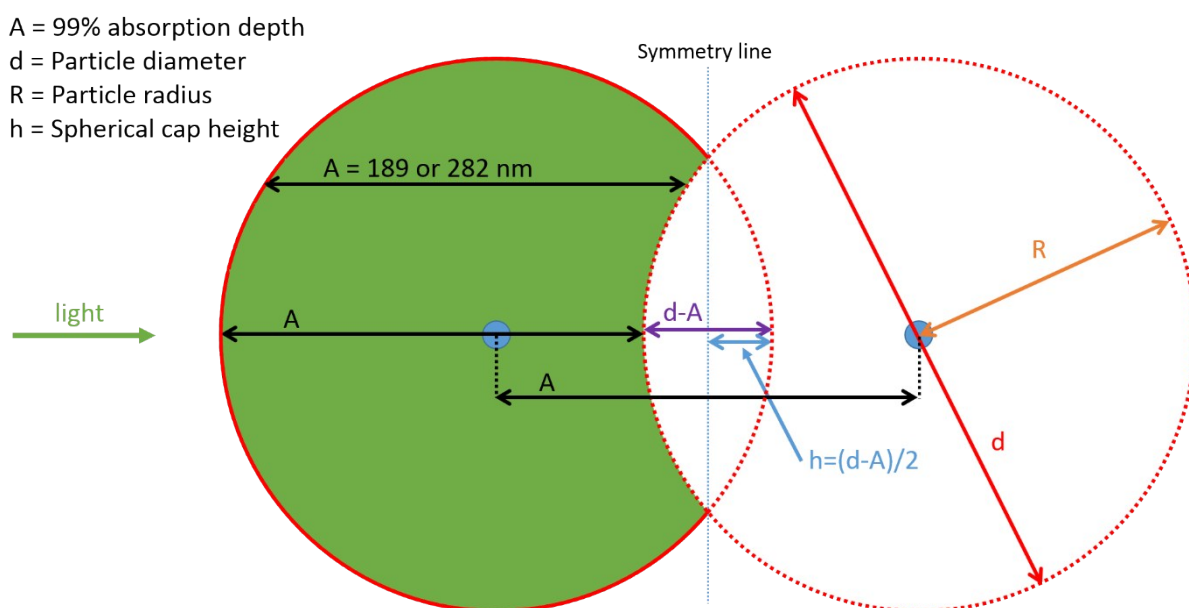


**Figure S-25.** Schematic detailing the geometry involved in estimating how much of the volume of a particle of a given size is actively absorbing during UV-vis measurements, based on the "99% absorption depths" calculated from the data in **Figure S-20** and **Figure S-24** (189 and 282 nm for **FS-TEG** and **FS-Hex** respectively).

**Table S-4.** Details of the estimated water/methanol/TEA dispersion number distributions.

	<b>Polymer</b>	<b>0.20 <math>\mu\text{m}</math></b>	<b>0.45 <math>\mu\text{m}</math></b>	<b>1.0 <math>\mu\text{m}</math></b>	<b>1.5 <math>\mu\text{m}</math></b>	<b>Totals</b>
<b>100 – Transmittance (420 nm)</b>	FS-Hex	0.27	1.63	9.99	20.05	-
	FS-TEG	4.27	5.43	30.38	70.66	-
<b>Absorbing volume per particle</b>	FS-Hex	4	39	216	492	-
	FS-TEG	4	28	147	332	-
<b>Relative number of particles</b>	FS-Hex	6.4	3.5	3.9	2.0	15.8
	FS-TEG	102.4	4.1	17.0	12.1	135.6
<b>% Number of particles</b>	FS-Hex	40.4	22.2	24.5	12.9	-
	FS-TEG	75.5	3.0	12.5	8.9	-

The “100-Transmittance” and “% number of particles” quantities have units of percent, the absorbing volume per particle is given in units of ( $\text{nm}^3 \times 10^6$ ) and the “relative number of particles” has no units. Values that are discussed in the main text are shown in red.

## 9. Contact Angle Measurements

**Table S-5.** Contact angle measurements of all polymers with H<sub>2</sub>O.

<b>Polymer</b>	<b>CA (H<sub>2</sub>O) / °</b>
FP-Me <sup>b</sup>	94.0 ± 8.0
FP-Hex <sup>a</sup>	92.8 ± 0.6
FP-EtHex <sup>a</sup>	94.7 ± 0.3
FP-Oct <sup>a</sup>	101.4 ± 0.6
FP-Dodec <sup>a</sup>	99.4 ± 0.5
FP-TEG <sup>a</sup>	72.0 ± 1.0
FS-Me <sup>b</sup>	77.0 ± 3.0
FS-Hex <sup>a</sup>	83.0 ± 4.0
FS-EtHex <sup>a</sup>	86.4 ± 1.2
FS-Oct <sup>a</sup>	90.2 ± 0.4
FS-Dodec <sup>a</sup>	109 ± 2.7
FS-TEG <sup>a</sup>	69.6 ± 0.3

[a] Measured for films of the polymers drop cast from chloroform solution on glass.

[b] Measured for pressed pellet of the polymer.

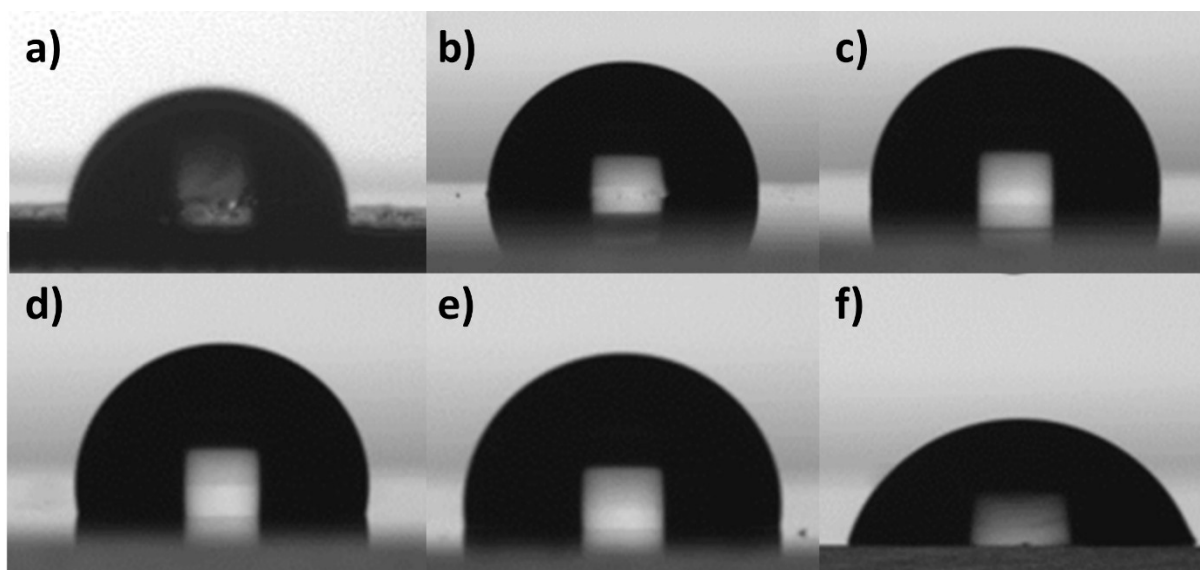


**Figure S-26.** Images of water droplets used for contact angles measurements on cast films of FP polymers apart from FP-Me which was measured on a pellet. a) FP-Me, b) FP-Hex, c) FP-EtHex, d) FP-Oct, e) FP-Dodec, f) FP-TEG.

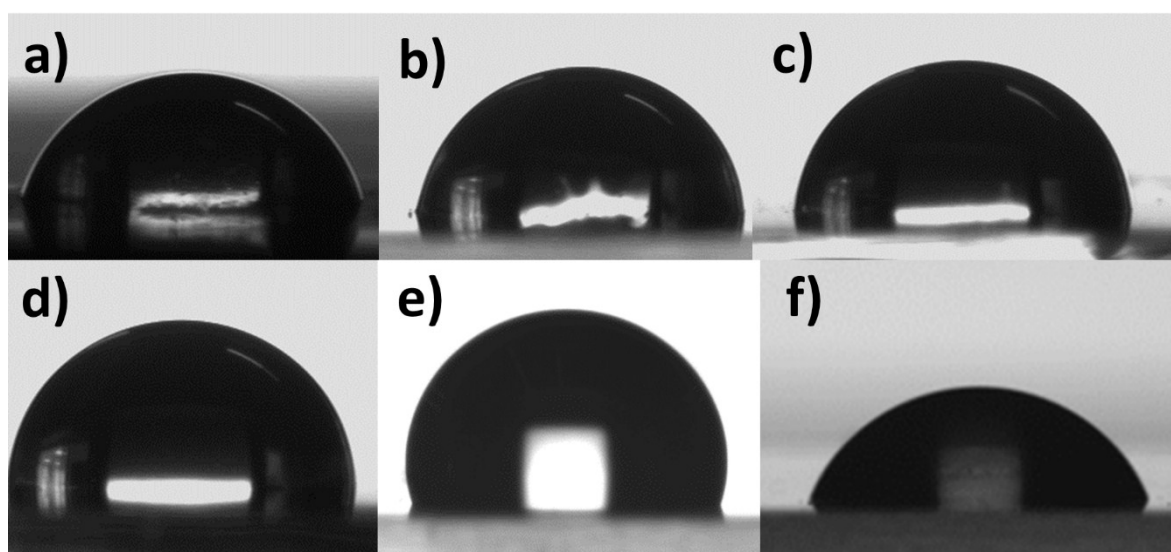


**Figure S-27.** Images of water droplets used for contact angles measurements on cast films of FS polymers apart from FS-Me which was measured on a pellet. a) FS-Me, b) FS-Hex, c) FS-EtHex, d) FS-Oct, e) FS-Dodec, f) FS-TEG.



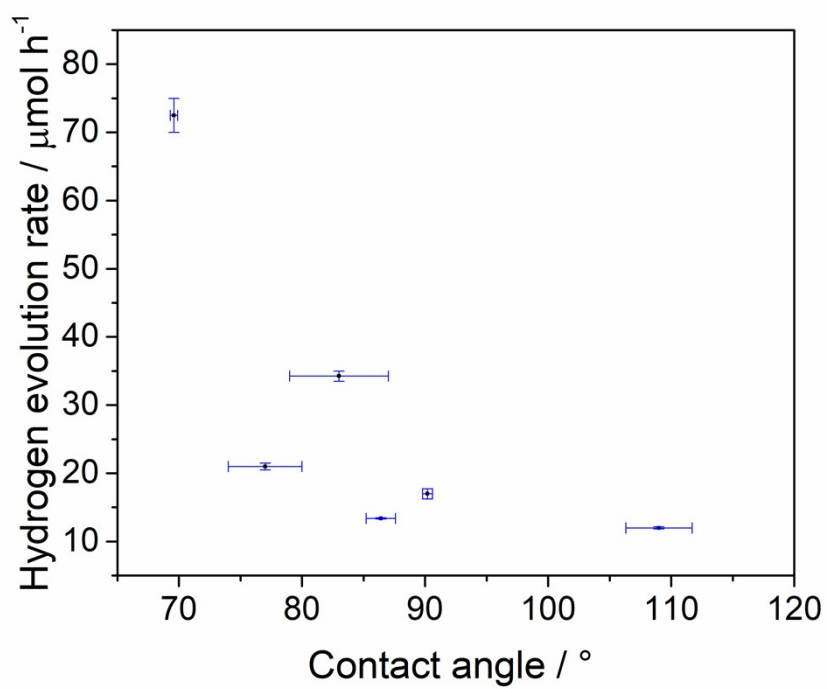


**Figure S-28.** Hydrogen evolution rates of the **FS** series plotted against their observed contact angles with water

## 10. Nitrogen Sorption Isotherms

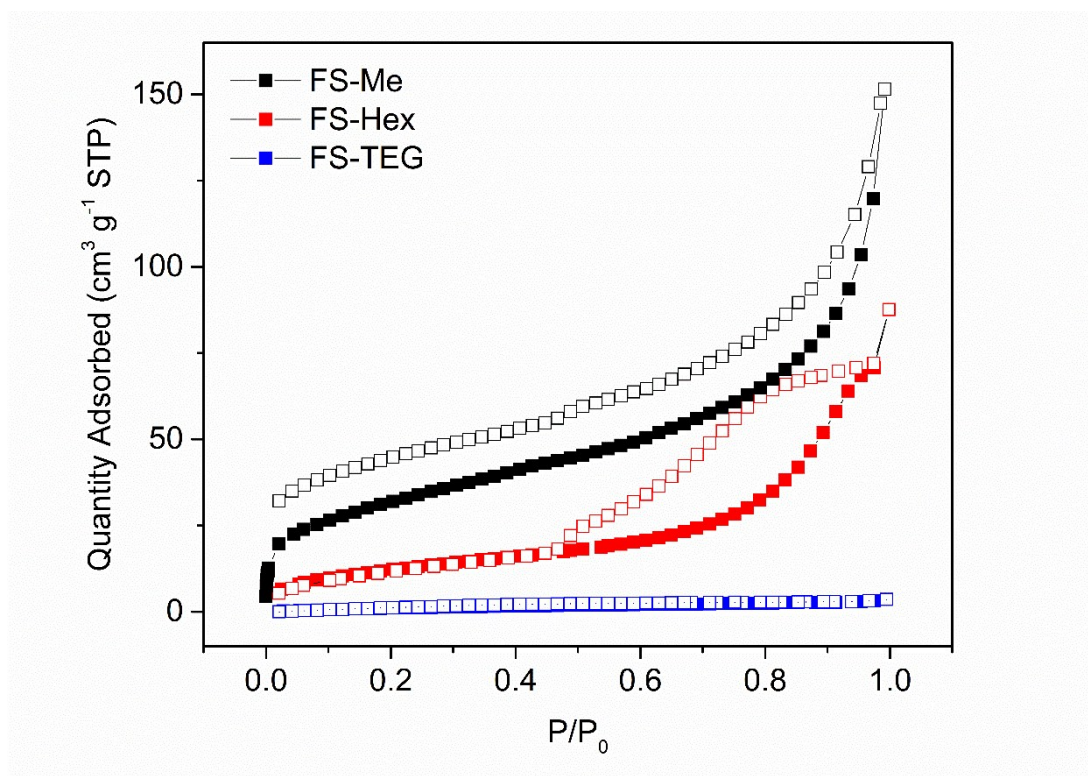


**Figure S-29.** Nitrogen sorption isotherm for **FS-Me**, **FS-Hex** and **FS-TEG** measured at 77.3 K and up to 1 bar (desorption curves shown as open symbols).

## 11. Atomic force microscopy measurements

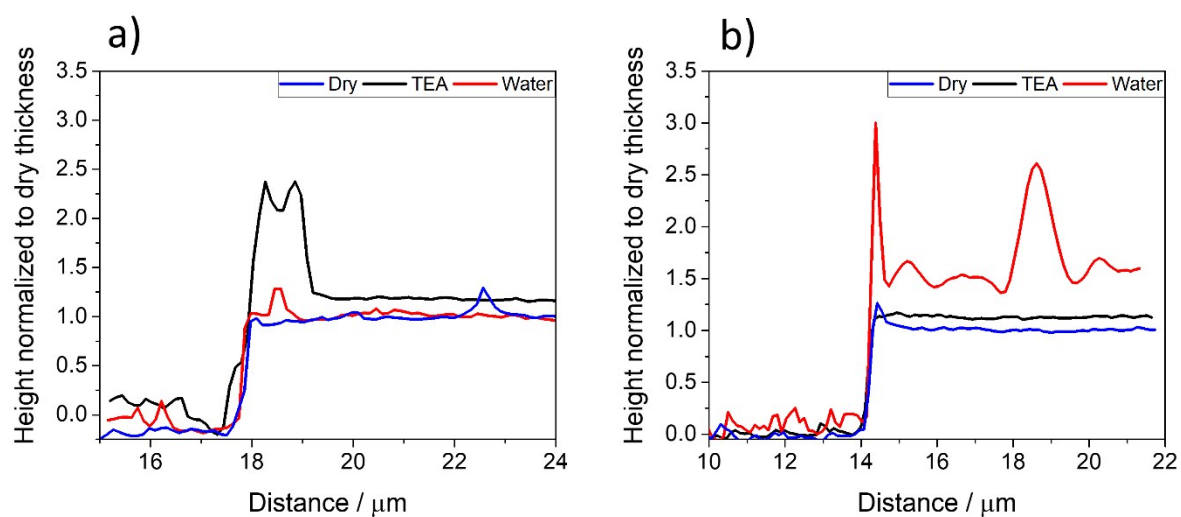


**Figure S-30.** Representative normalized thickness profiles of a) **FS-Hex** and b) **FS-TEG** as dry films and in contact with water and in contact with TEA, measured by atomic force microscopy.

## 12. Quartz Crystal Microbalance Measurements

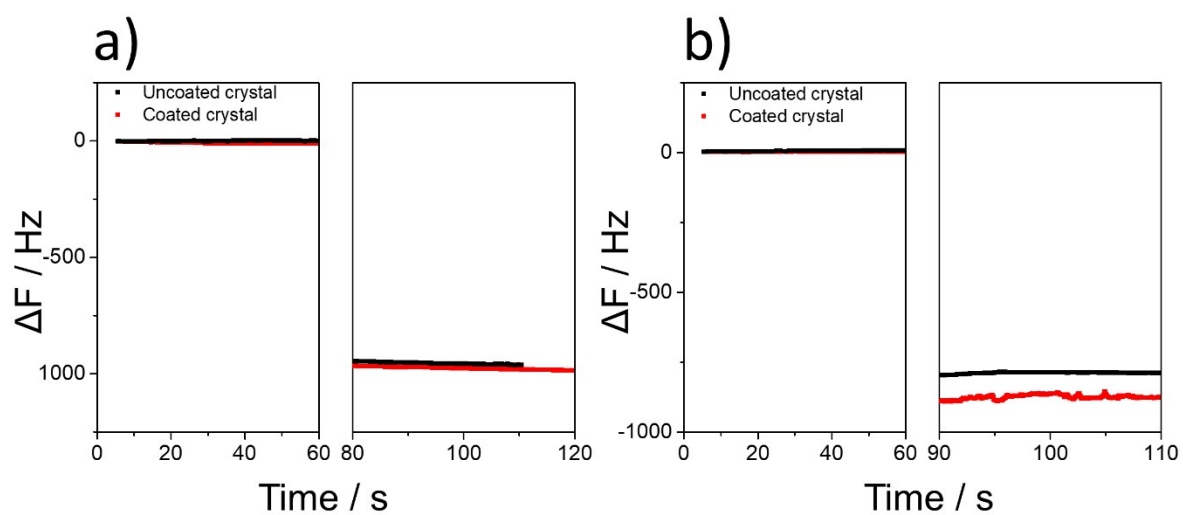


**Figure S-31.** QCM data showing the frequency of the bare crystal and crystal coated with a) **FS-Hex** and b) **FS-TEG**. Initial frequencies are obtained in air before a step change takes place upon submersion in water.

### 13. Photoelectron Spectroscopy in Air (PESA)

Table S-6. Photoelectron spectroscopy in air data for polymer thin-films.

Material	UV Intensity / nW	Workfunction <sup>a</sup> / eV	PESA-inferred ionization potentials vs. SHE <sup>b</sup> / eV
FP-Hex	50	5.81	+ 1.37
FP-TEG	50	5.53	+ 1.09
FS-Hex	60	5.81	+ 1.37
FS-Oct	80	5.96	+ 1.52
FS-Dodec	90	5.97	+ 1.53
FS-TEG	50	5.68	+ 1.24

[a] Workfunctions recorded using a Riken Keiki PESA spectrometer (Model AC-2) with a power number of 0.33. Samples for PESA were prepared on glass substrates. [b] Obtained from workfunction – 4.44 eV.

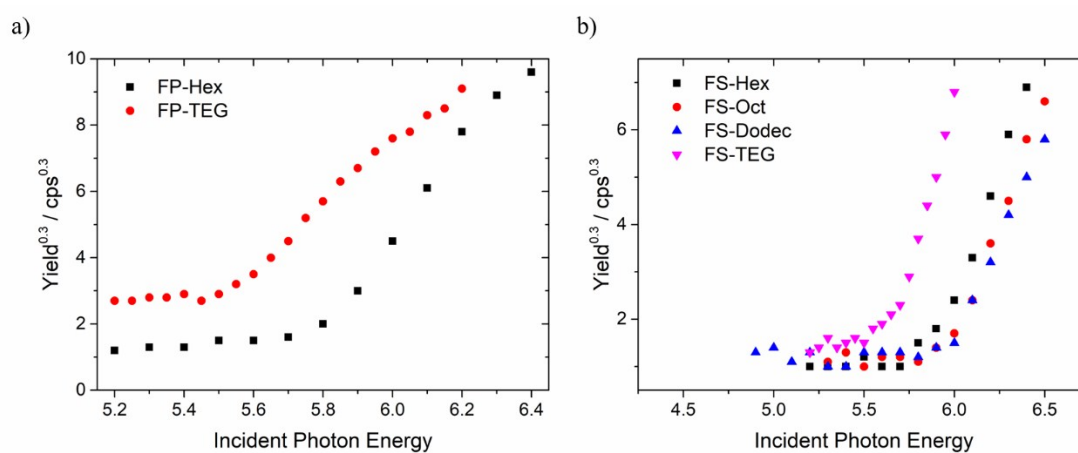
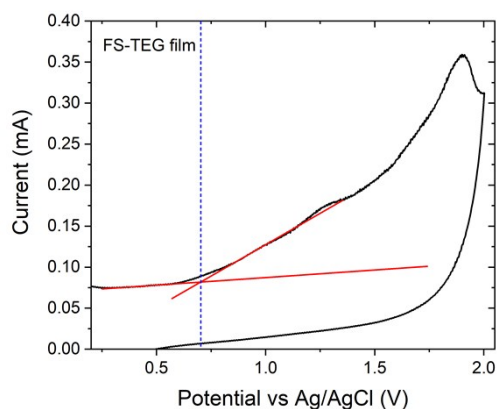


Figure S-32. PESA traces of a) FP polymers and b) FS polymers.

## 14. Cyclic Voltammetry



**Figure S-33.** Cyclic voltammetry of a **FS-TEG** polymer film. The ionization potential (i.e. the oxidation potential) was calculated by extrapolating the onset of the oxidative current to the current baseline (intercept of red lines). **FS-TEG** has an ionization potential of  $-5.3 \pm 0.2$  V versus vacuum when immersed in a high dielectric environment. This potential is, within error, in agreement with our DFT calculations in water. Note that potentials are expected to be similar in water and in acetonitrile.<sup>16</sup>

**Table S-7.** Summary of the ionization potentials determined by voltammetry.

Potentials	vs $E_{Ag/AgCl}$	$E_{SHE}^{Ag/AgCl}$	vs $E_{vacuum}$
	/ V <sup>a</sup>	/ V <sup>b</sup>	/ V <sup>a</sup>
<b>FS-TEG</b>	0.703	0.143	-5.286

[a] Ionization potentials versus Ag/AgCl as measured and versus vacuum respectively. [b] Potential of the Ag/AgCl reference electrode versus the standard hydrogen electrode.

**Table S-8.** Comparison of measured and calculated ionization potentials in this work.

Potentials	FS-TEG	FS-Me
	/ V	/ V
<b>CV (<math>\epsilon_r = 37.5</math>)</b>	-5.3	-
<b>DFT (<math>\epsilon_r = 80.1</math>)</b>	-	-5.4

Note: All values have an error of  $\pm 0.2$  V.

## 15. Hydrogen Evolution

**Table S-9.** Hydrogen evolution performance of all polymers in suspension.<sup>a</sup>

Polymer	HER <sup>b</sup>	
	$\lambda > 420 \text{ nm} / \mu\text{mol g}^{-1} \text{ h}^{-1}$	$\lambda > 420 \text{ nm} / \mu\text{mol mmol}^{-1} \text{ h}^{-1}$
FP-Me	$8.3 \pm 0.2$	$2.3 \pm 0.1$
FP-Hex	0	0
FP-EtHex	$4.3 \pm 0.2$	$2.0 \pm 0.1$
FP-Oct	$5.2 \pm 0.3$	$2.4 \pm 0.1$
FP-Dodec	$6 \pm 1$	$4 \pm 1$
FP-TEG	$306 \pm 6$	$163 \pm 3$
FS-Me	$840 \pm 20$	$340 \pm 10$
FS-Hex	$1370 \pm 20$	$750 \pm 20$
FS-EtHex	$535 \pm 3$	$323 \pm 2$
FS-Oct	$680 \pm 7$	$410 \pm 20$
FS-Dodec	$479 \pm 6$	$343 \pm 4$
FS-TEG	$2,900 \pm 100$	$1,980 \pm 70$

[a] Reaction conditions: 25 mg of the polymer was suspended in 22.5 mL of a water/methanol/triethylamine solution (1:1:1 ratio), irradiated by 300 W Xe light source fitted with a  $\lambda > 420 \text{ nm}$  band pass filter. [b] Rate normalized per gram of polymer [c] Rate normalized to the molecular weight of each polymer's repeating unit.

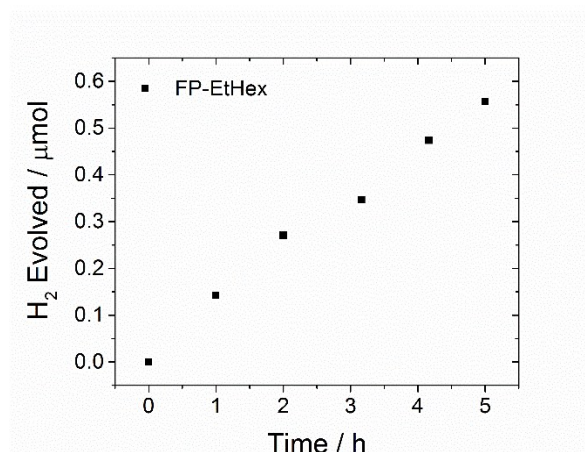


**Figure S-34.** Hydrogen evolution of **FP-EtHex** (25 mg) from a water/methanol/triethylamine mixture under  $\lambda > 420 \text{ nm}$  irradiation (300 W Xe light source).

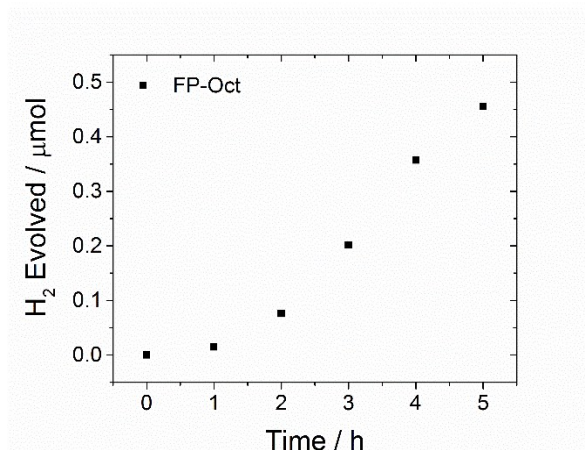


**Figure S-35.** Hydrogen evolution of **FP-Oct** (25 mg) from a water/methanol/triethylamine mixture under  $\lambda > 420$  nm irradiation (300 W Xe light source).

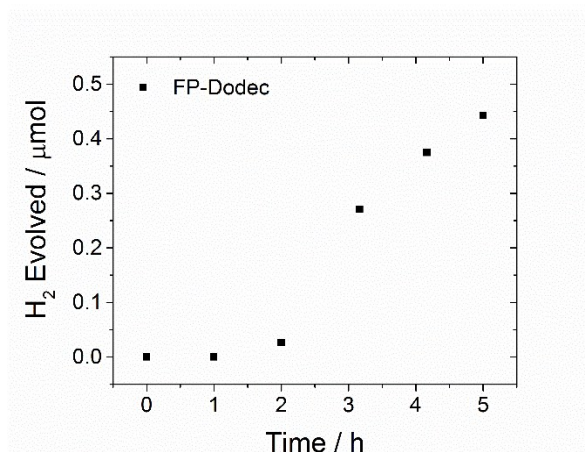


**Figure S-36.** Hydrogen evolution of **FP-Dodec** (25 mg) from a water/methanol/triethylamine mixture under  $\lambda > 420$  nm irradiation (300 W Xe light source).

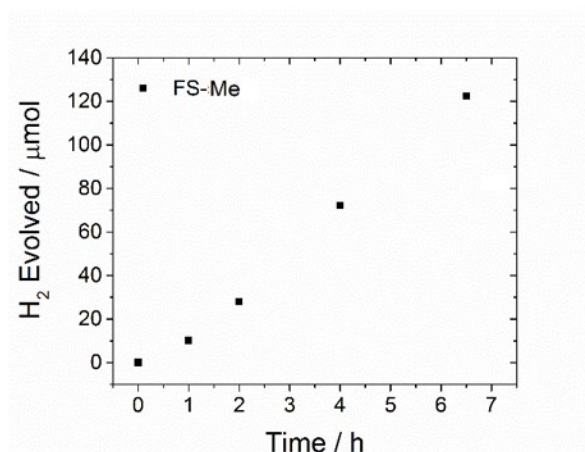


**Figure S-37.** Hydrogen evolution of **FS-Me** (25 mg) from a water/methanol/triethylamine mixture under  $\lambda > 420$  nm irradiation (300 W Xe light source).

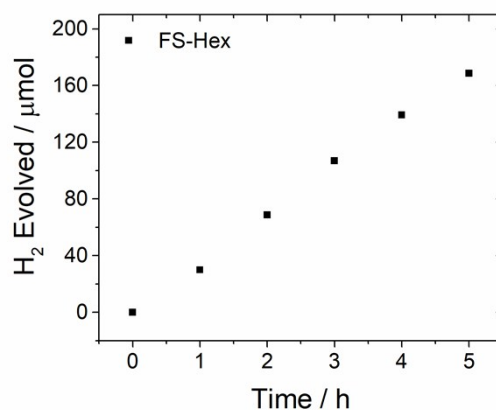


**Figure S-38.** Hydrogen evolution of **FS-Hex** (25 mg) from a water/methanol/triethylamine mixture under  $\lambda > 420$  nm irradiation (300 W Xe light source).

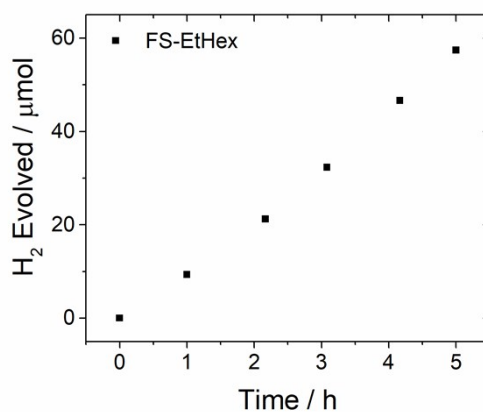


**Figure S-39.** Hydrogen evolution of **FS-EtHex** (25 mg) from a water/methanol/triethylamine mixture under  $\lambda > 420$  nm irradiation (300 W Xe light source).

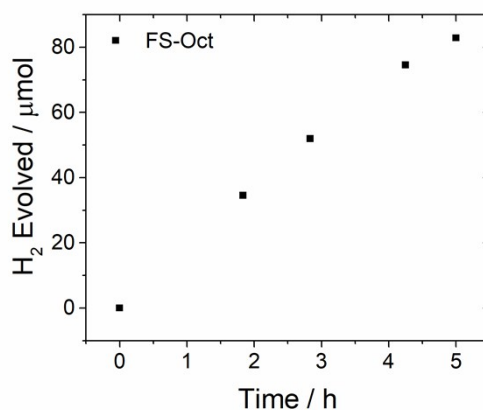


**Figure S-40.** Hydrogen evolution of **FS-Oct** (25 mg) from a water/methanol/triethylamine mixture under  $\lambda > 420$  nm irradiation (300 W Xe light source).



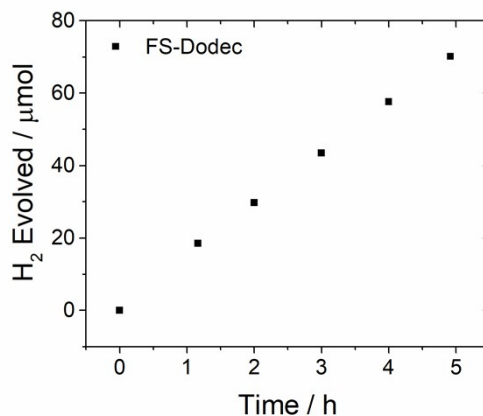


**Figure S-41.** Hydrogen evolution of **FS-Dodec** (25 mg) from a water/methanol/triethylamine mixture under  $\lambda > 420$  nm irradiation (300 W Xe light source).

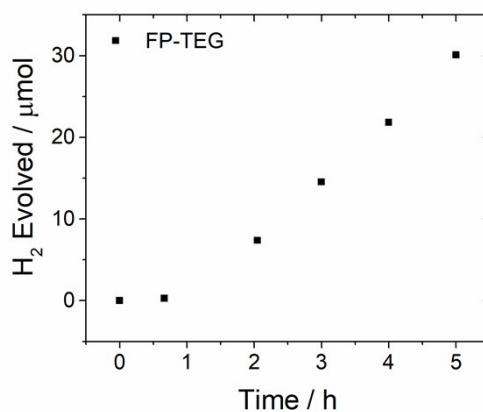


**Figure S-42.** Hydrogen evolution of **FP-TEG** (25 mg) from a water/methanol/triethylamine mixture under  $\lambda > 420$  nm irradiation (300 W Xe light source).

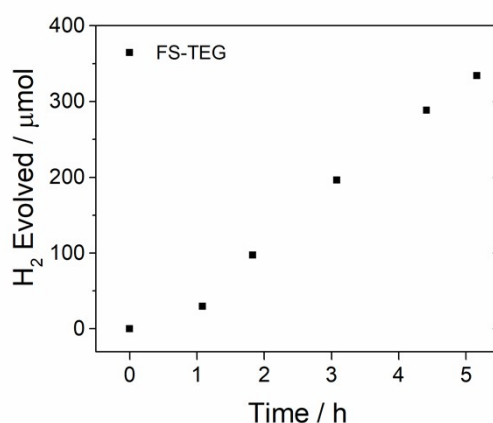


**Figure S-43.** Hydrogen evolution of **FS-TEG** (25 mg) from a water/methanol/triethylamine mixture under  $\lambda > 420$  nm irradiation (300 W Xe light source).

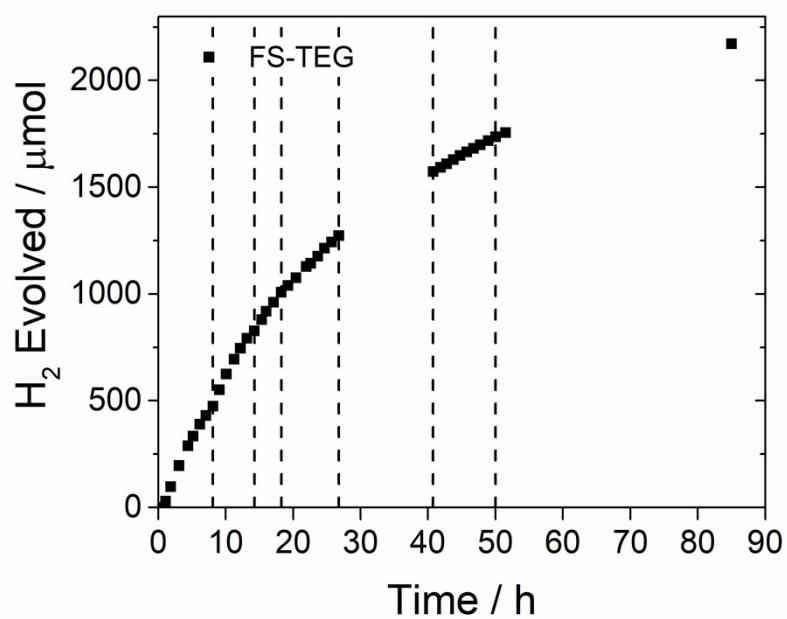


**Figure S-44.** Hydrogen evolution of **FS-TEG** (25 mg) from a water/methanol/triethylamine mixture under  $\lambda > 420$  nm irradiation (300 W Xe light source) over a 90-hour period with intermittent degassing (dashed lines).

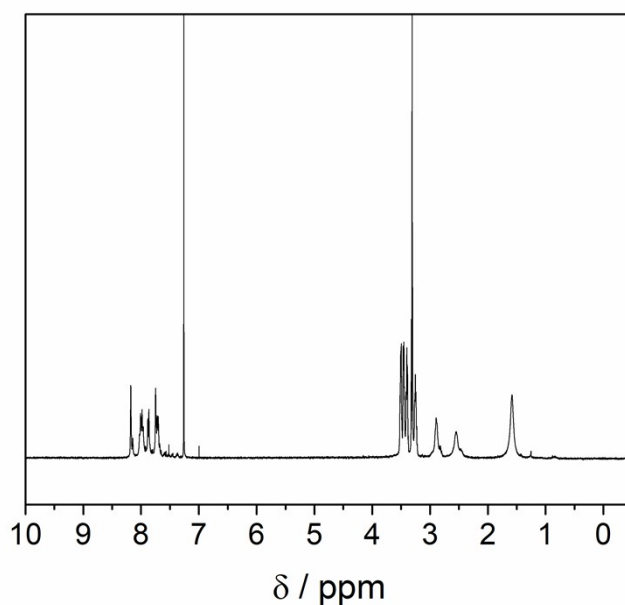


**Figure S-45.** <sup>1</sup>H NMR spectrum of the free-standing film of **FS-TEG** after the extended photocatalysis experiment.

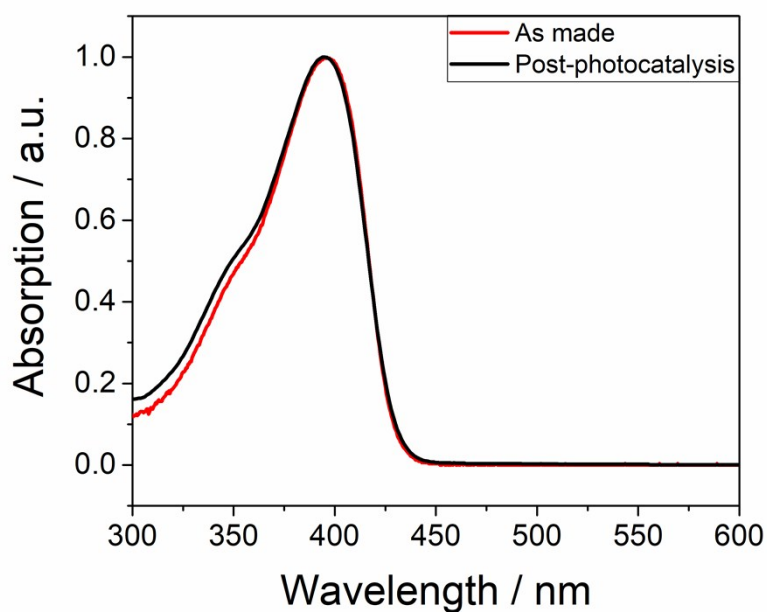


**Figure S-46.** UV-Vis spectrum of the free-standing film of **FS-TEG** after the extended photocatalysis experiment compared to the as made material. Both measurements were performed in chloroform solution.

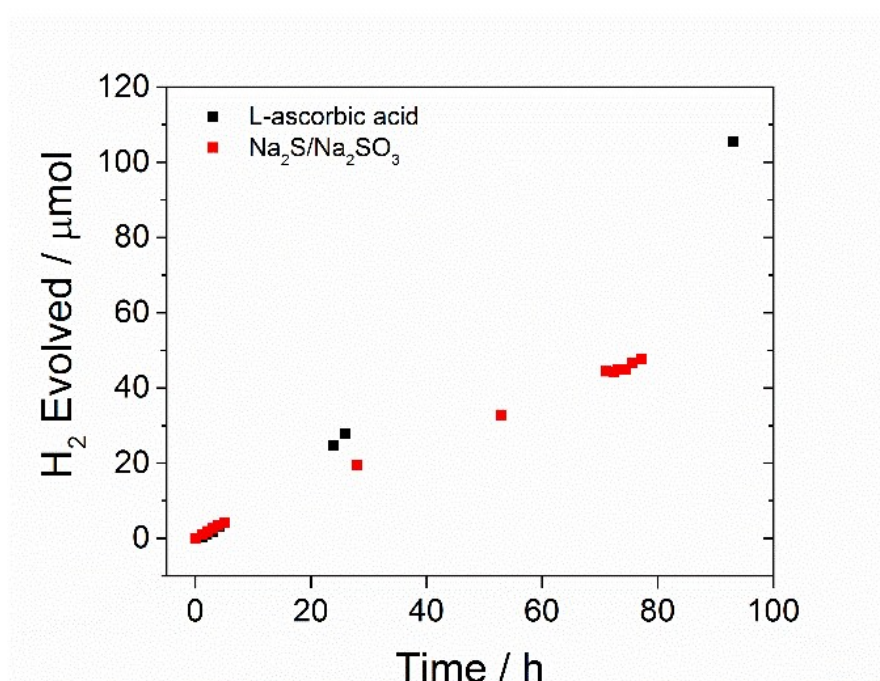


**Figure S-47.** Hydrogen evolution of **FS-TEG** (25 mg) from solutions of L-ascorbic acid (0.2 M) and sodium sulfide/sodium sulfite (0.35 M / 0.25 M) under  $\lambda > 420$  nm irradiation (300 W Xe light source).

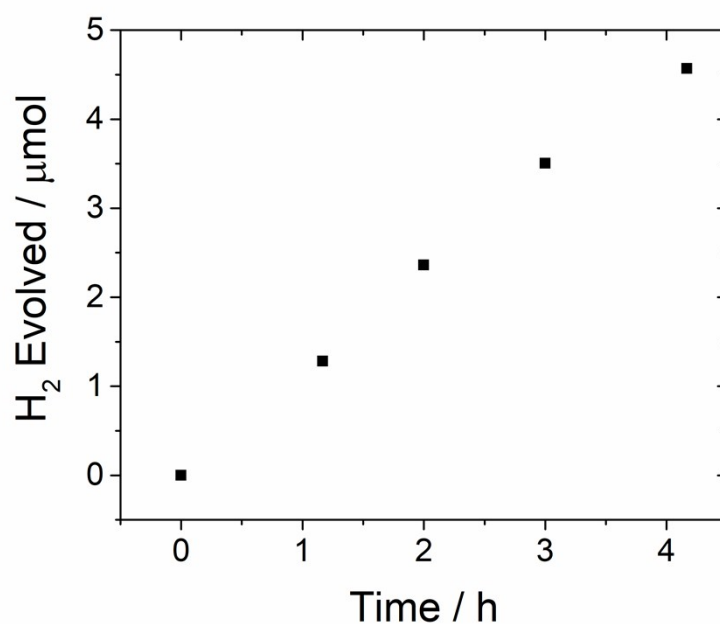


**Figure S-48.** Hydrogen evolution of a film of **FS-TEG** spin-coated from 3 mg mL<sup>-1</sup> solutions of chloroform onto a roughened glass slide. Film placed in 5 vol.% TEA mixture under  $\lambda > 420$  nm irradiation (300 W Xe light source).

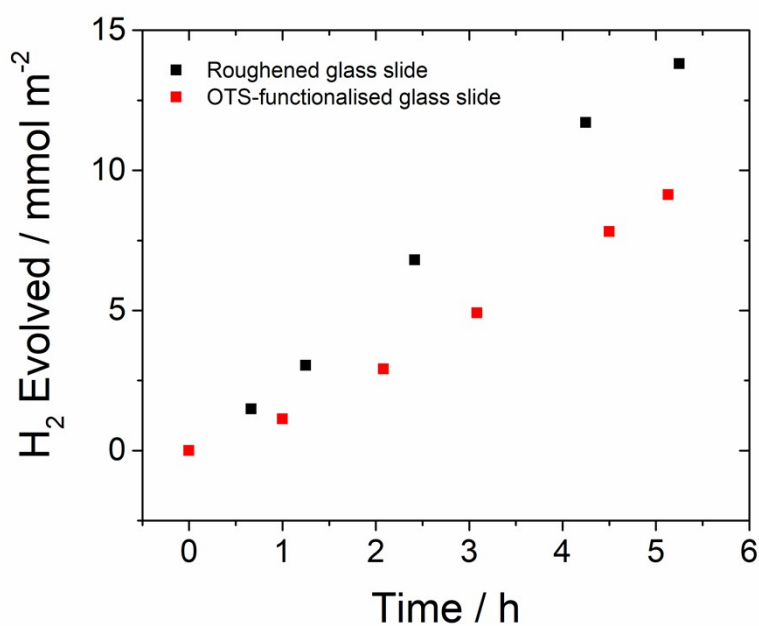


**Figure S-49.** Hydrogen evolution of films of **FS-TEG** spin-coated from 10 mg mL<sup>-1</sup> solutions of chloroform onto a roughened glass slide and an OTS-functionalised slide. Films placed in 5 vol. % TEA mixture under  $\lambda > 420$  nm irradiation (300 W Xe light source).

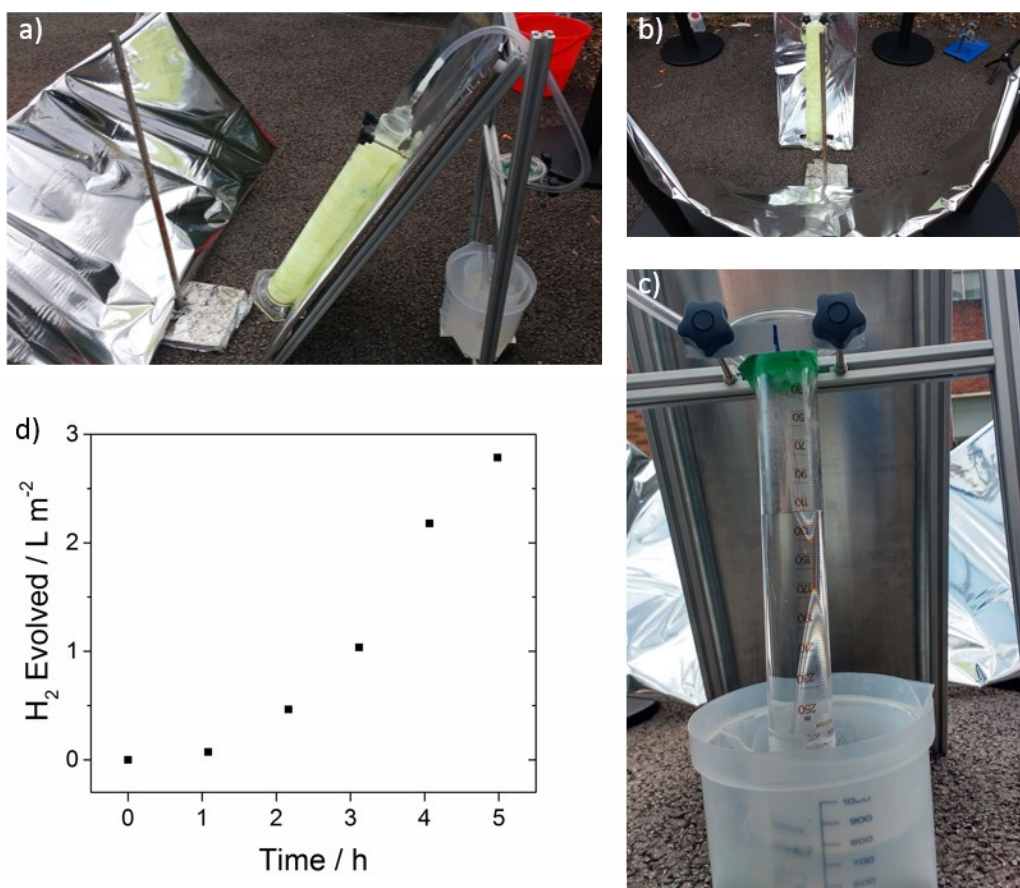


**Figure S-50.** a) Side-view of photoreactor set-up with reflective panel and polymer-coated glass fibers submerged in 5 vol. % TEA connected to a hydrogen collection vessel (right) b) Front view of photoreactor set-up c) Back view of hydrogen collection vessel d) Amount of hydrogen evolved over a 5-hour period on a largely overcast day.

## 16. Wavelength Dependent Hydrogen Evolution Experiments

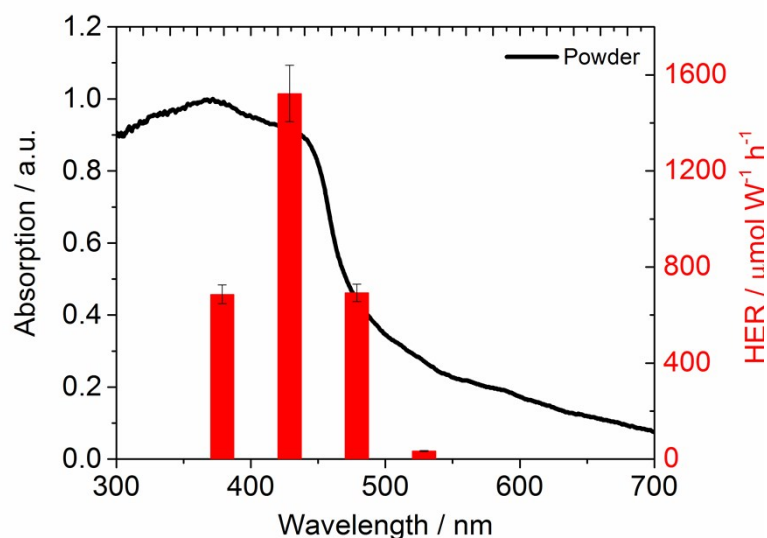


**Figure S-51.** Hydrogen evolution of powdered FS-TEG (10.2 mg) from 5 vol. % TEA/water under  $\lambda = 370, 420, 470$  and  $520$  nm irradiation plotted with UV-vis absorption spectra of powdered FS-TEG.

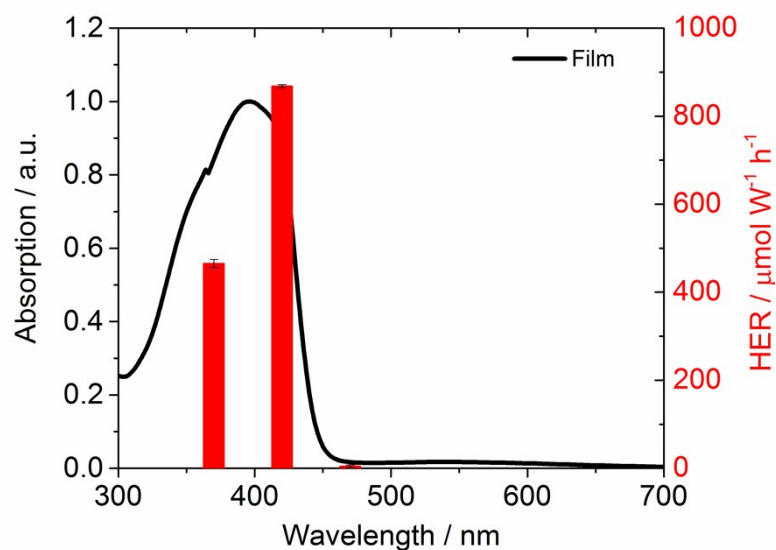


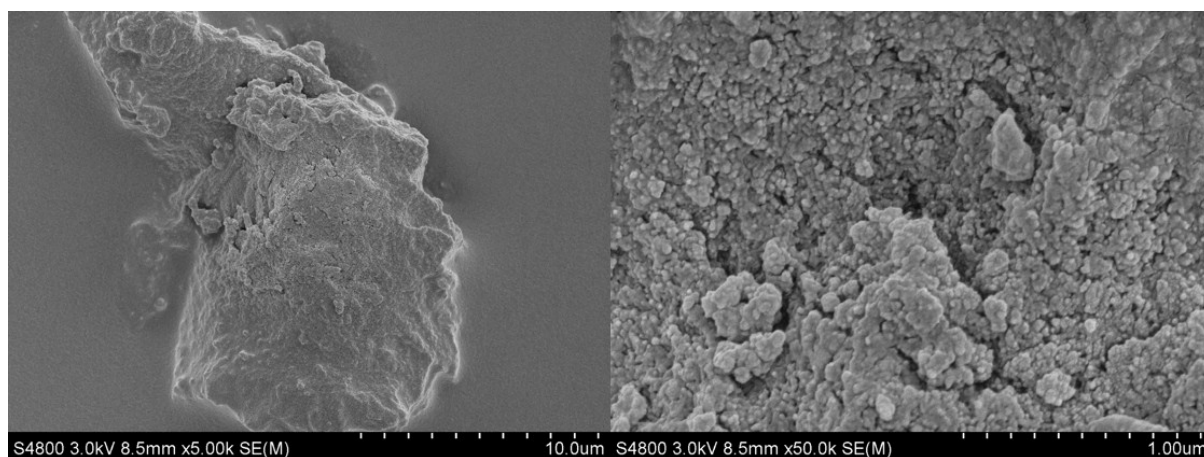
**Figure S-52.** Hydrogen evolution of FS-TEG film drop cast on roughened glass from 5 vol.% TEA under  $\lambda = 370, 420$  and  $470$  nm irradiation plotted with UV-vis absorption spectra of the film.

## 17. Film Thickness Measurements

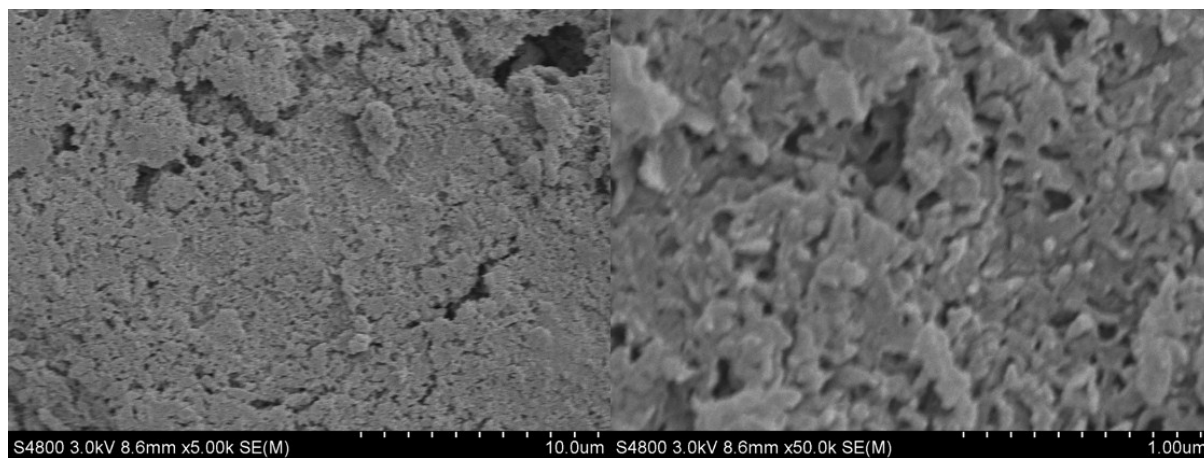
**Table S-10.** Thicknesses of FS-TEG films spin-coated on OTS-functionalised glass slides from various concentrations of chloroform obtained by AFM and profilometry.

Concentration / mg mL <sup>-1</sup>	Thickness / nm	
	AFM	Profilometry
1	11.3 ± 0.2	-
3	19.9 ± 0.2	-
5	36 ± 4	-
10	81 ± 8	79 ± 3
15	-	113 ± 4

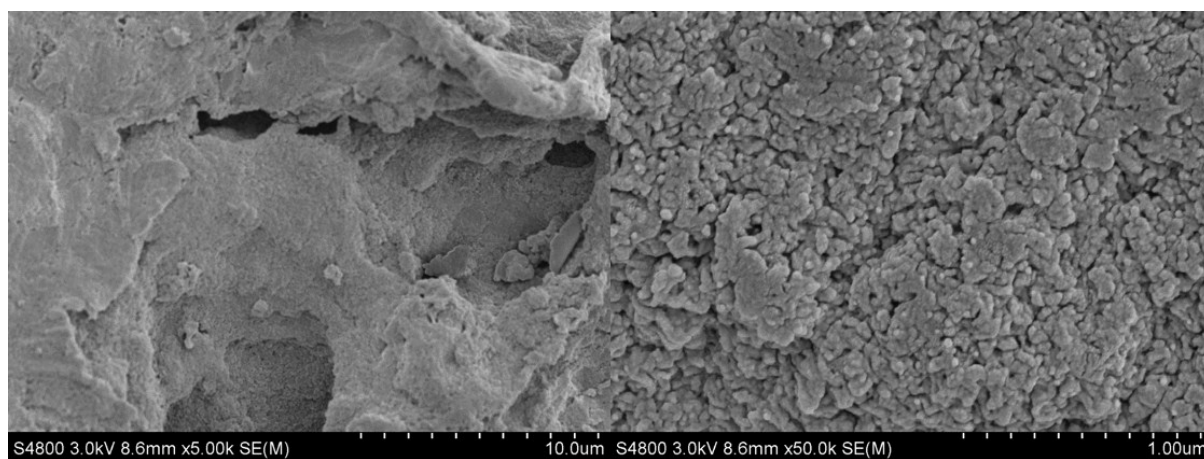
## 18. Scanning Electron Microscopy



**Figure S-53.** SEM images of **FS-Hex** powder.

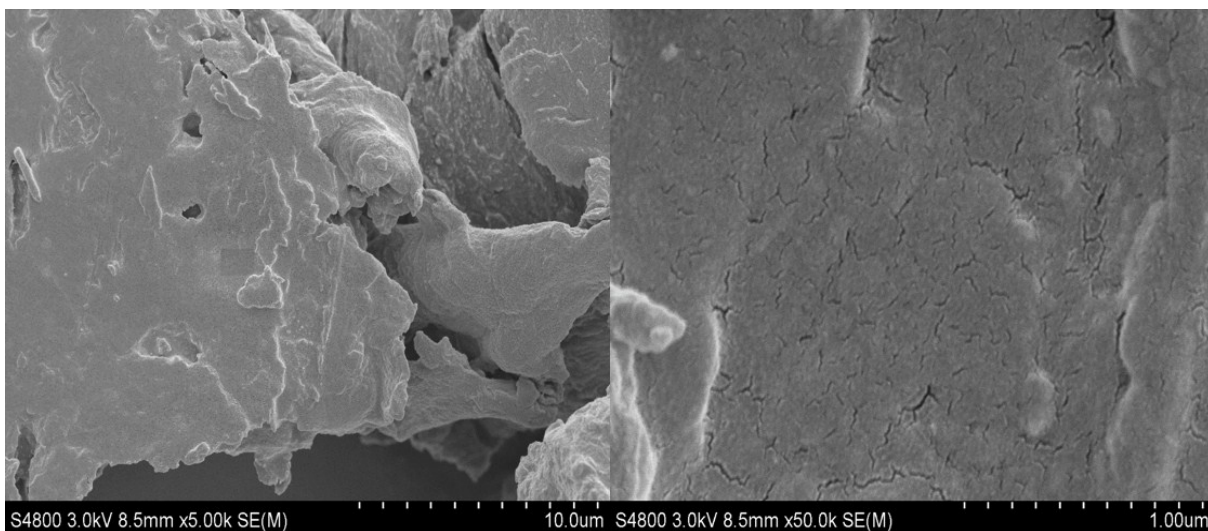


**Figure S-54.** SEM images of **FS-Oct** powder.

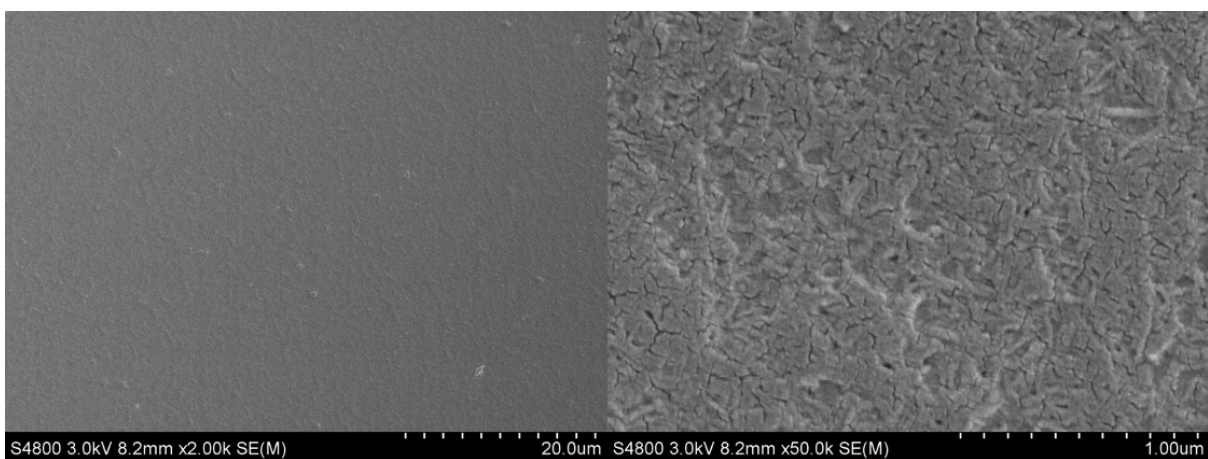


**Figure S-55.** SEM images of **FS-Dodec** powder.

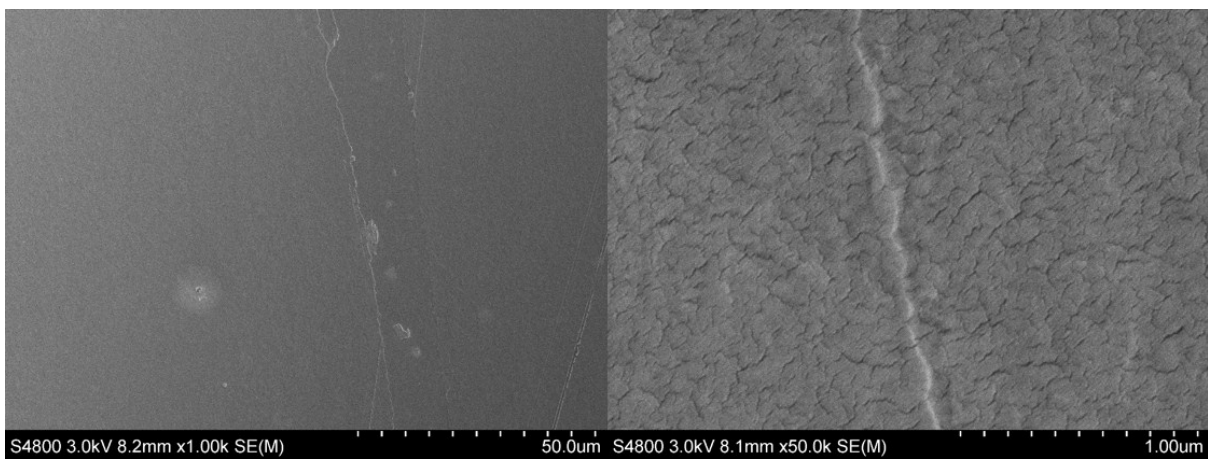




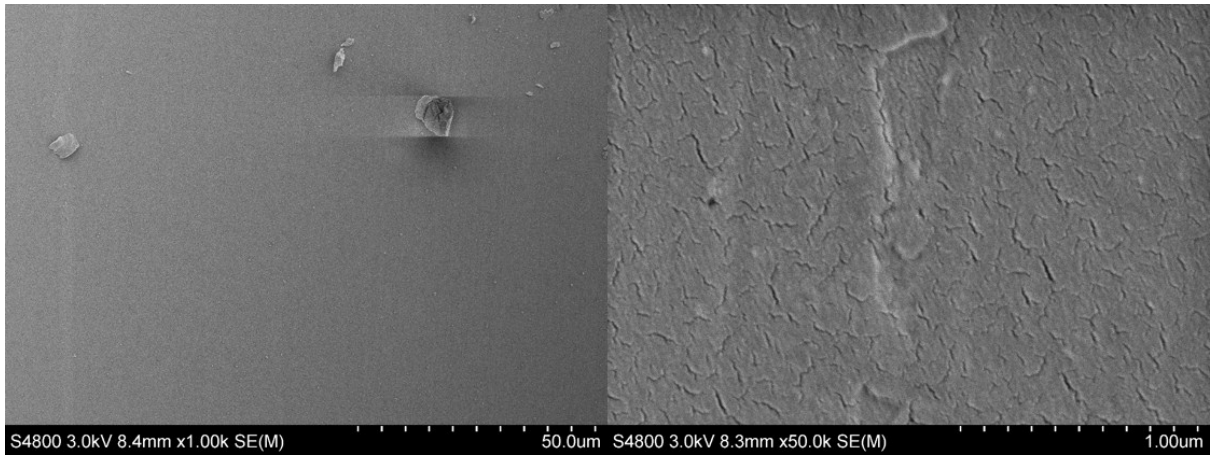
**Figure S-56.** SEM images of **FS-TEG** powder.



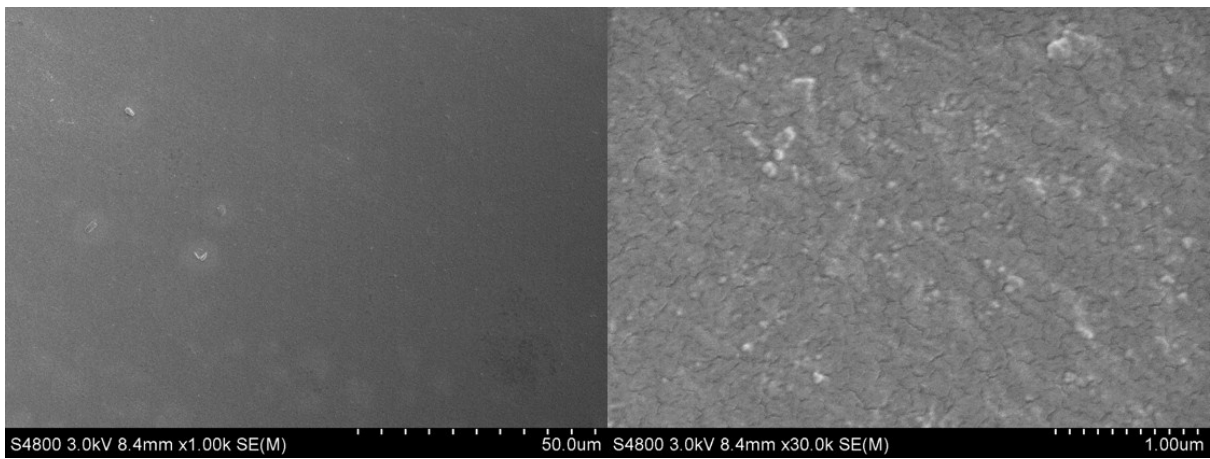
**Figure S-57.** SEM images of **FS-Hex** film drop casted from chloroform.



**Figure S-58.** SEM images of **FS-Oct** film drop casted from chloroform.



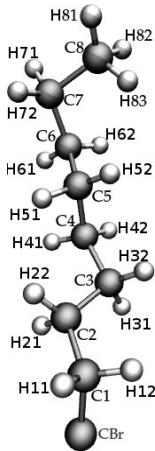
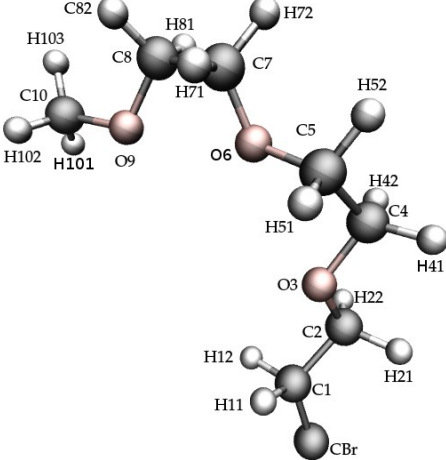
**Figure S-59.** SEM images of **FS-Dodec** film drop casted from chloroform.



**Figure S-60.** SEM images of **FS-TEG** film drop casted from chloroform.

## 19. Molecular Dynamics

**Table S-11.** Forcefield Parameters for the sidechains used in this work.

					
<u>Atom</u>	<u>Partial Charge (e)</u>	<u>OPLS Type</u>	<u>Atom</u>	<u>Partial Charge (e)</u>	<u>OPLS Type</u>
CBr	+0.360	opls_145	CBr	+0.260	opls_145
C1	-0.355	opls_139	C1	-0.246	opls_139
C2	-0.060	opls_139	C2	+0.013	opls_139
C3	-0.120	opls_139	O3	-0.383	opls_179
C3	-0.120	opls_139	C4	+0.005	opls_139
C5	-0.120	opls_139	C5	+0.009	opls_139
C6	-0.120	opls_139	O6	-0.383	opls_179
C7	-0.120	opls_139	C7	+0.009	opls_139
C8	-0.180	opls_139	C8	+0.002	opls_139
All H	+0.060	opls_140	O9	-0.383	opls_179
			C10	-0.049	opls_139
			All H	+0.090	opls_140

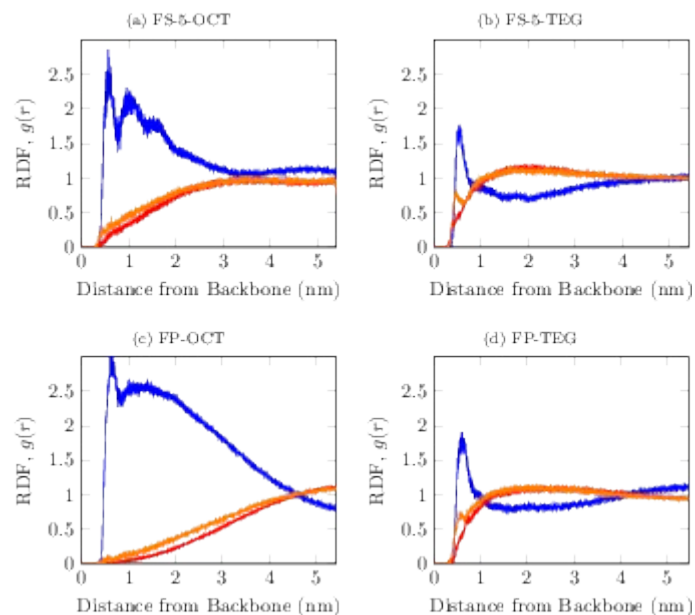


**Figure S-61.** Molecular dynamics radial distribution functions (RDFs) of the oligomers in the reaction mixture. Blue, Red and Orange represent TEA, water and methanol, respectively.

## 20. Transient Absorption Spectroscopy

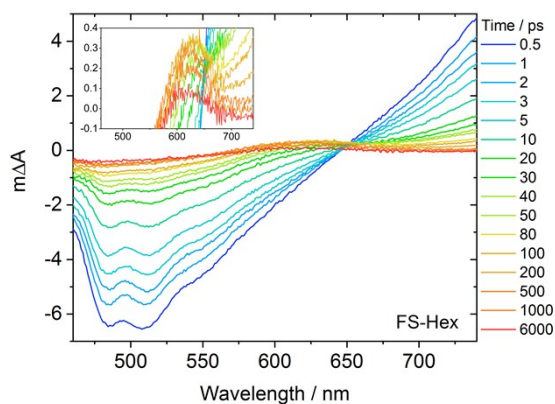


**Figure S-62.** fs-TAS spectrum of a **FS-Hex** dispersion measured from 0.5 ps to 6 ns after excitation at 420 nm. The 0.2 mg mL<sup>-1</sup> water/methanol/TEA samples were measured under identical fluences of 87  $\mu\text{J cm}^{-2}$  in a 2 mm cuvette. Inset: Magnified spectra highlighting the 600 nm absorption feature.

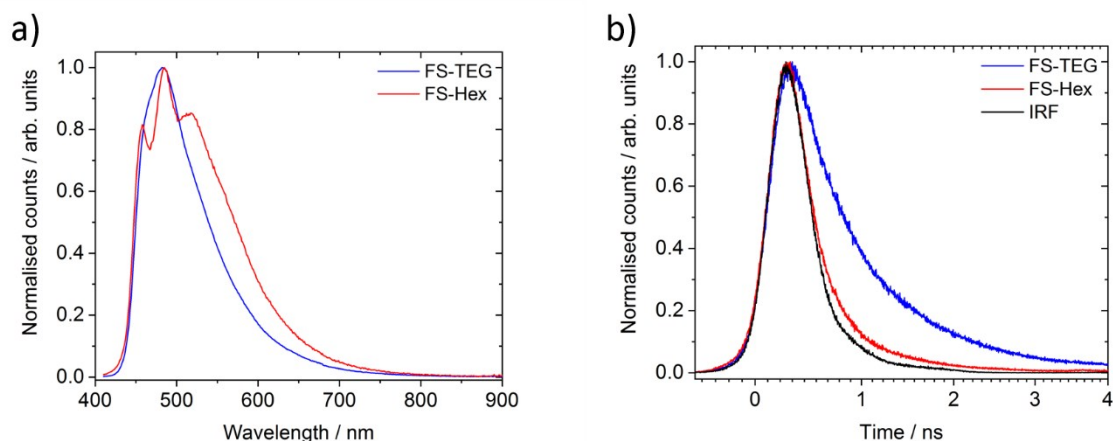


**Figure S-63.** (a) Normalized photoluminescence spectra and (b) TCSPC exciton lifetimes of  $0.02 \text{ mg mL}^{-1}$  **FS-TEG** and **FS-Hex** dispersions in water/methanol/TEA, measured in a 2 mm cuvette with a FLS1000 PL spectrometer. IRF = Instrument response function.

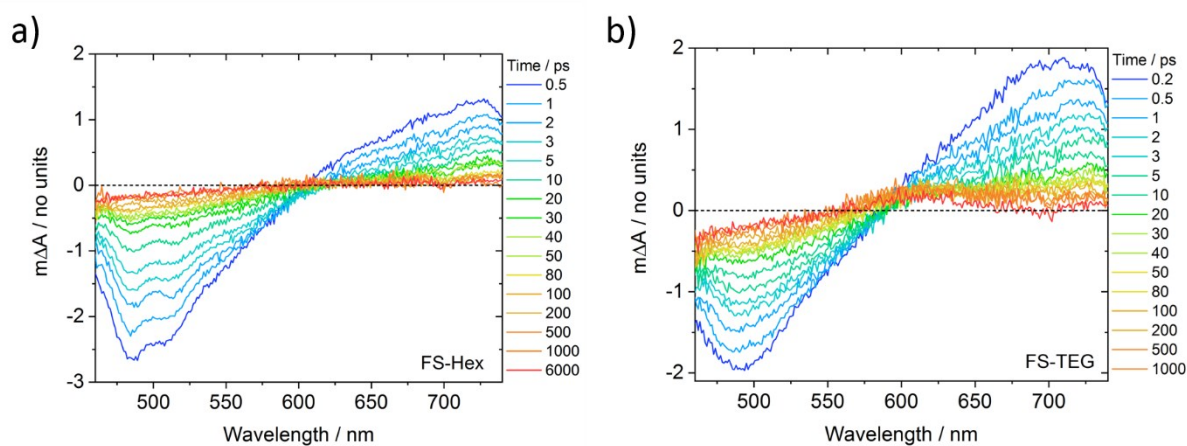


**Figure S-64.** fs-TAS spectra of (a) **FS-Hex** and (b) **FS-TEG** dispersions in 1:1 vol.% water/methanol mixtures. These samples were made at a concentration of  $0.02 \text{ mg mL}^{-1}$  and measured in a 10 mm quartz cuvette. The same excitation fluence of  $102 \mu\text{J cm}^{-2}$  was used in both cases.



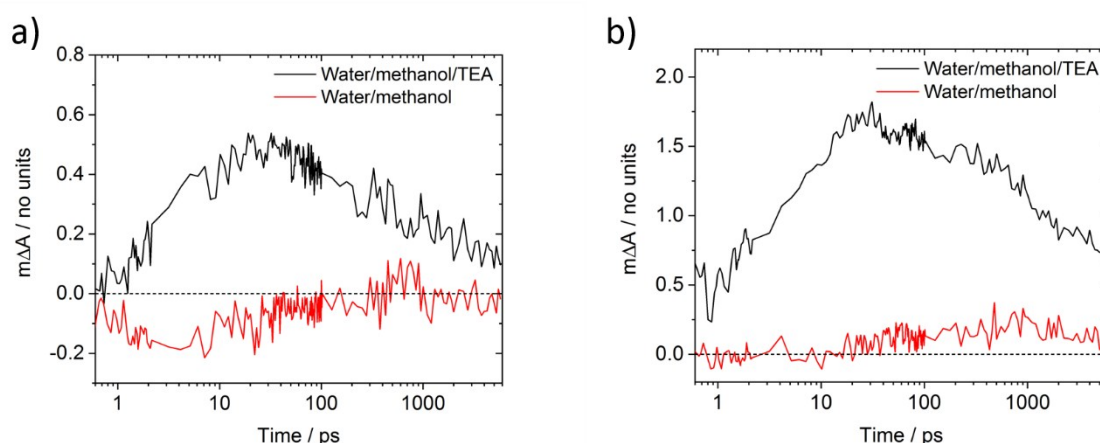


**Figure S-65.** fs-TAS 600 nm electron kinetics of (a) **FS-Hex** and (b) **FS-TEG** dispersions in equal parts 4 at 0.5 ps from all subsequent times. The effect of TEA as a hole scavenger can clearly be seen. These samples were made at a concentration of  $0.02 \text{ mg mL}^{-1}$  and measured in a 10 mm quartz cuvette. The same excitation fluence of  $102 \mu\text{J cm}^{-2}$  was used in both cases.

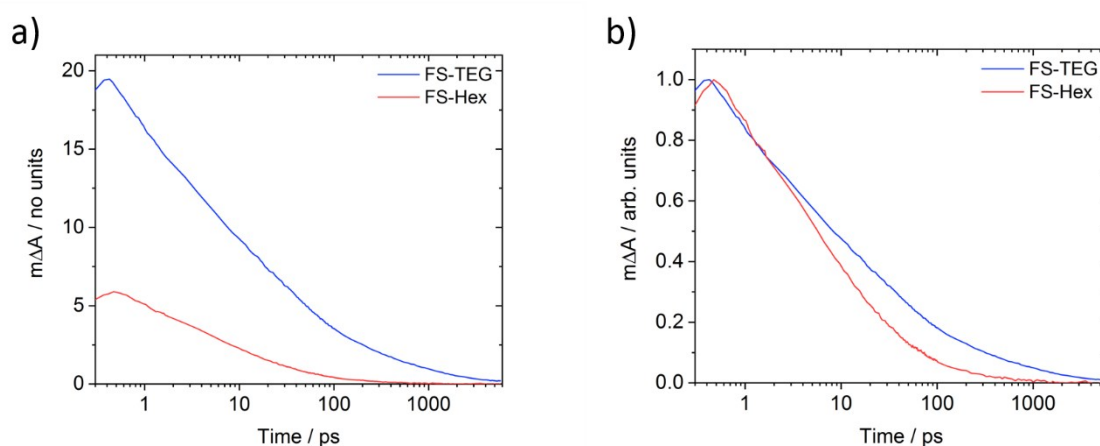


**Figure S-66.** fs-TAS exciton kinetics of **FS-Hex** and **FS-TEG** dispersions in water/methanol/TEA, probed at 750 nm after excitation at 420 nm. (a) As measured (b) Normalized for comparison of kinetics. The  $0.2 \text{ mg mL}^{-1}$  water/methanol/TEA samples were measured under identical fluences of  $87 \mu\text{J cm}^{-2}$  in a 2 mm cuvette.

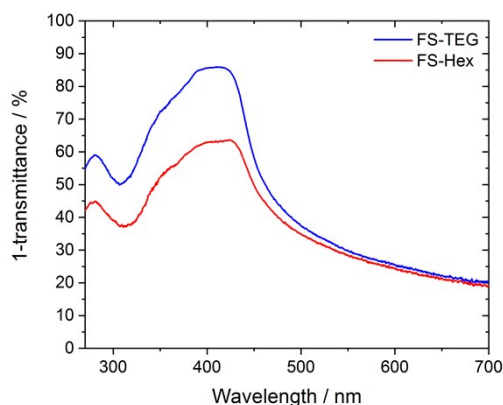


**Figure S-67.** Representative 1-Transmittance spectra of **FS-Hex** and **FS-TEG** femtosecond TAS samples ( $0.2 \text{ mg mL}^{-1}$  in water/methanol/TEA, 2 mm cuvette).

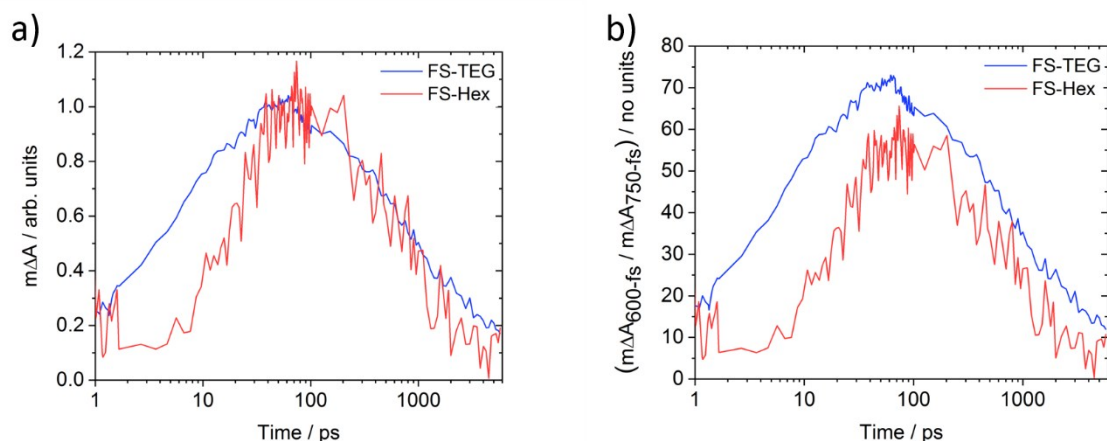


**Figure S-68.** fs-TAS electron kinetics of **FS-Hex** and **FS-TEG** dispersions in water/methanol/TEA (a) Normalized by their respective maxima for a comparison of kinetics (b) normalized by the maximum difference in absorption at 750 nm (i.e. by the number of photogenerated excitons). These kinetics were probed at 600 nm after excitation at 420 nm. Samples were made at a concentration of  $0.2 \text{ mg mL}^{-1}$  and measured in a 2 mm quartz cuvette. The same excitation fluence of  $87 \mu\text{J cm}^{-2}$  was used in both cases.

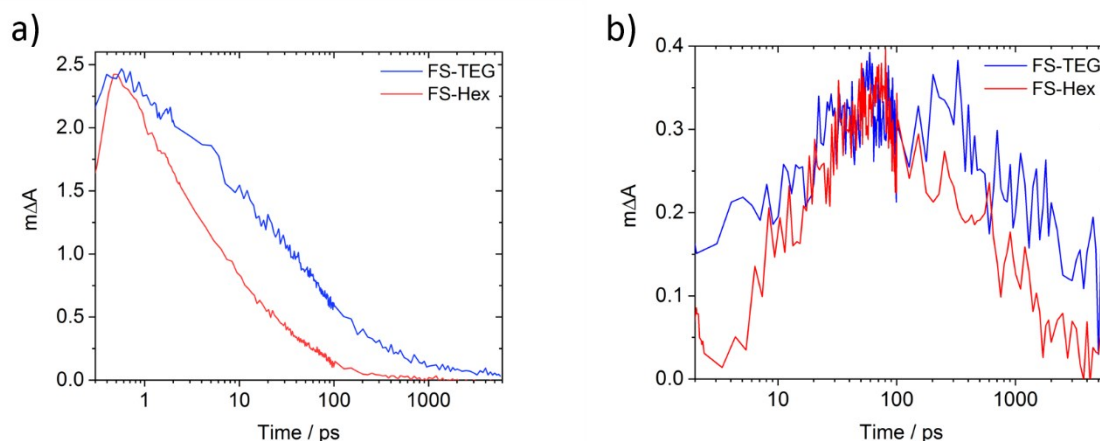


**Figure S-69.** Comparison of kinetics when **FS-Hex** and **FS-TEG** dispersions in water/methanol/TEA are excited at different fluences such that their maximum exciton densities (*i.e.* maximum  $\Delta A$  at 725 nm) are the same. Here **FS-Hex** was excited at  $102 \mu\text{J cm}^{-2}$  and **FS-TEG** was excited at  $13 \mu\text{J cm}^{-2}$ . (a) Comparison of exciton kinetics at 725 nm, showing the stabilisation of the exciton in **FS-TEG** relative to **FS-Hex**. (b) Comparison of deconvoluted 600 nm electron kinetics, calculated by subtracting the shape of the TAS spectrum at 0.5 ps, at which point only excitons have formed, from all subsequent times.

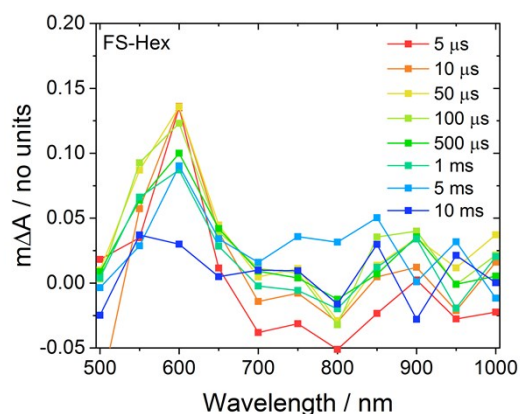


**Figure S-70.**  $\mu\text{s}$ -TAS spectrum of a **FS-Hex** dispersion in  $0.02 \text{ mg mL}^{-1}$  water/methanol/TEA, taken under identical conditions to the **FS-TEG** spectrum in the main text. A 10 mm cuvette was used. The excitation fluence was  $0.92 \text{ mJ cm}^{-2}$ .



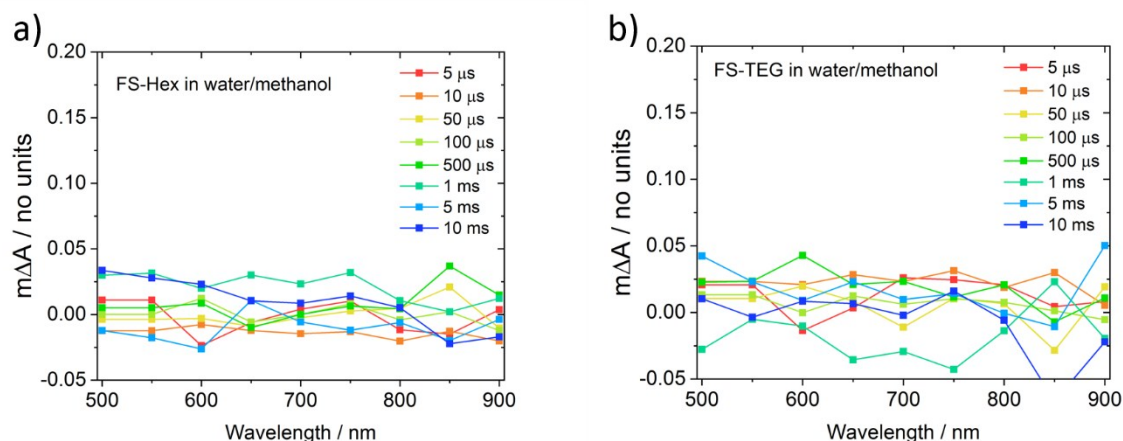


**Figure S-71.**  $\mu$ s-TAS of  $0.02 \text{ mg mL}^{-1}$  dispersions of (a) **FS-Hex** and (b) **FS-TEG** in water/methanol. In both cases, there are no spectral features. A 10 mm cuvette was used. The excitation fluence was  $0.92 \text{ mJ cm}^{-2}$ .

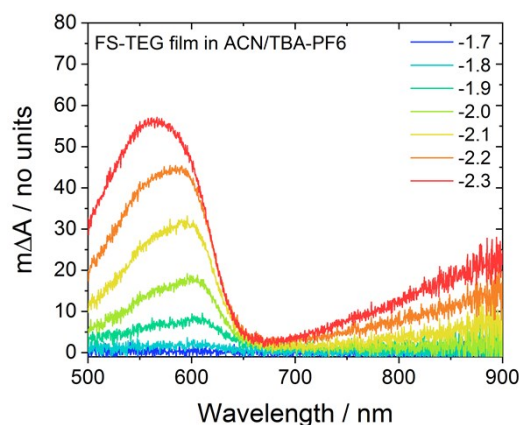


**Figure S-72.** Difference between the steady-state absorption spectra of an **FS-TEG** film under negative bias and the spectrum of a film at open circuit. At  $-1.7 \text{ V}$  vs  $\text{Ag}/\text{AgCl}$ , the absorption spectrum is identical to the unbiased absorption spectrum. At potentials beyond  $-1.7 \text{ V}$ , formation of the electron polaron causes absorption at  $550\text{-}600 \text{ nm}$  and also in the near infra-red, in good agreement with TAS spectra of polymers dispersed in water/methanol/TEA. The linear sweep voltammetry was applied at a scan rate of  $100 \text{ mVs}^{-1}$ . Absorbance spectra were taken every second using a white light probe.

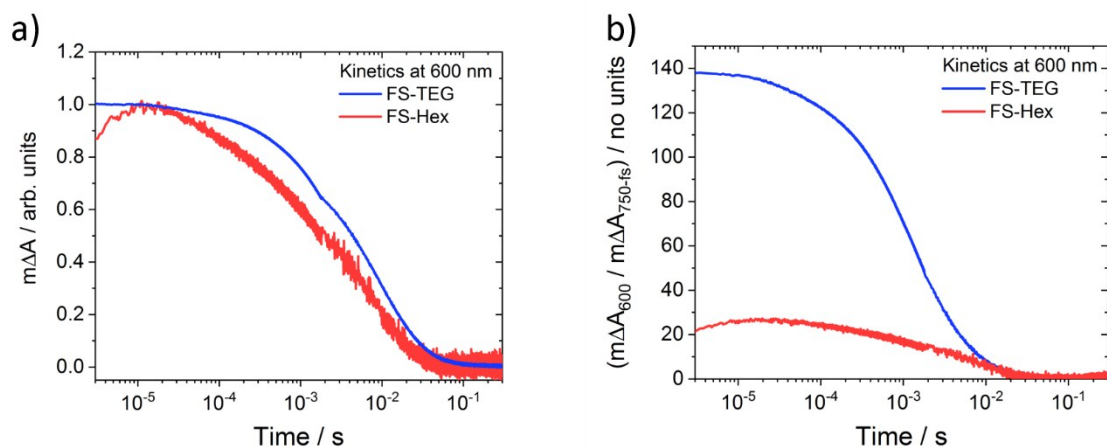


**Figure S-73.**  $\mu\text{s}$ -TAS 600 nm kinetics of  $0.02 \text{ mg mL}^{-1}$  **FS-Hex** and **FS-TEG** dispersions in water/methanol/TEA. (a) Normalised for comparison of lifetimes. (b) Normalised by the maximum absorption difference measured at 750 nm in the fs-TAS (i.e. by the number of initial photoexcited states). Both samples were excited at  $0.92 \text{ mJ cm}^{-2}$  with 420 nm light in 10 mm cuvettes.

**Table S-12.** Summary of exciton and electron half-lives in **FS-Hex** and **FS-TEG** water/methanol/TEA dispersions, measured by fs-TAS.

<b>fs-TAS</b>	<b>Fluence</b> <b>/ <math>\mu\text{J cm}^{-2}</math></b>	<b>Polymer</b>	<b>Exciton half-life</b> <b>/ ps</b>	<b>Electron half-life</b> <b>/ ps</b>
<b>Same</b>	87	FS-Hex	5.6	852
<b>fluence</b>	87	FS-TEG	8.7	952
<b>Different</b>	102	FS-Hex	4.4	652
<b>fluence</b>	13	FS-TEG	22.1	2000

**Table S-13.** Summary of electron half-lives in **FS-Hex** and **FS-TEG** water/methanol/TEA dispersions, measured by  $\mu\text{s}$ -TAS.

<b><math>\mu\text{s}</math>-TAS</b>	<b>Fluence</b> <b>/ <math>\text{mJ cm}^{-2}</math></b>	<b>Polymer</b>	<b>Electron half-life</b> <b>/ ms</b>
<b>Same</b>	0.92	FS-Hex	2.0
<b>fluence</b>	0.92	FS-TEG	4.4
<b>Different</b>	1.49	FS-Hex	1.1
<b>fluence</b>	0.02	FS-TEG	22.8

## 21. Previous Literature Reports on Polymer Photocatalysts

**Table S-14.** Comparison of the photocatalytic activity of FS-TEG compared to other reports.

Polymer	Processability	EQE / % @420 nm	HER / $\mu\text{mol h}^{-1}$	Conditions	Reference
P1	None	0.4 @420 nm	1.6	25 mg photocatalyst, $\lambda > 420$ nm, 300 W Xe light source, H <sub>2</sub> O/MeOH/TEA, atmospheric pressure	17
P10	None	11.6 @420 nm	81.5	25 mg photocatalyst, $\lambda > 420$ nm, 300 W Xe light source, H <sub>2</sub> O/MeOH/TEA, atmospheric pressure	17
P64	None	20.7 @420 nm	151.0	25 mg photocatalyst, AM1.5g solar simulator, H <sub>2</sub> O/MeOH/TEA, atmospheric pressure	18
B-BT-1,4	None	4.01 @420 nm	116	50 mg photocatalyst loaded with Pt, $\lambda > 420$ nm, 300 W Xe light source, TEOA/H <sub>2</sub> O, reduced pressure	19
S-CMP3	None	13.2 @420 nm	78	25 mg photocatalyst, $\lambda > 420$ nm, 300 W Xe light source, H <sub>2</sub> O/MeOH/TEA, atmospheric pressure	20
CTF-15	None	15.9 @420 nm	48	25 mg photocatalyst loaded with Pt, $\lambda > 420$ nm, 300 W Xe light source, H <sub>2</sub> O/MeOH/TEA, atmospheric pressure	21
PCP4e	None	0.34 @350 nm	6.6	3.5 mg photocatalyst, $\lambda > 400$ nm, 150 W Xe light source, H <sub>2</sub> O/TEA, atmospheric pressure	22
PCP1-100%PDI	None	-	7.2	3.5 mg photocatalyst, $\lambda > 400$ nm, 150 W Xe light source, H <sub>2</sub> O/TEA, atmospheric pressure	23
ter-CTF-0.7	None	22.8 @420 nm	966	50 mg photocatalyst loaded with Pt, $\lambda > 420$ nm, 300 W Xe light source, TEOA/H <sub>2</sub> O, reduced pressure	24
PTO-300-5	None	5.5 @400 nm	10.8	10 mg photocatalyst loaded with Pt, $\lambda > 420$ nm, 300 W Xe light source, H <sub>2</sub> O/TEOA, atmospheric pressure	25
SNP-BTT1	None	4.5 @420 nm	47	15 mg photocatalyst loaded with Pt, $\lambda > 395$ nm, 300 W Xe light source, H <sub>2</sub> O/CAN/TEOA, atmospheric pressure	26
PTI	Nanosheets in water	1.3 @400 nm	3.5	3.6 mg photocatalyst loaded with Pt, $\lambda > 420$ nm, 300 W Xe light source, H <sub>2</sub> O/TEOA, atmospheric pressure	27
PTB7-Th/EH-IDTBR	Organic solvents	2.0 @400 nm, 6.2 @700 nm,	129	2 mg photocatalyst composite loaded with Pt, $350 > \lambda > 800$ nm, 300 W Xe light source, H <sub>2</sub> O/ascorbic acid, 100 Torr	28
P8s	Organic solvents	0.56 @420 nm	1.8	25 mg photocatalyst, $\lambda > 420$ nm, 300 W Xe light source, H <sub>2</sub> O/MeOH/TEA, atmospheric pressure	29
<b>FS-TEG</b>	<b>Organic solvents</b>	<b>10.0 @420 nm</b>	<b>72.5</b>	<b>25 mg photocatalyst, <math>\lambda &gt; 420</math> nm, 300 W Xe light source, H<sub>2</sub>O/MeOH/TEA, atmospheric pressure</b>	<b>This work</b>

## 22. References

- 1 J. M. Behrendt, Y. Wang, H. Willcock, L. Wall, M. C. McCairn, R. K. O'Reilly and M. L. Turner, *Polym. Chem.*, 2013, **4**, 1333–1336.
- 2 R. S. Sprick, B. Bonillo, R. Clowes, P. Guiglion, N. J. Brownbill, B. J. Slater, F. Blanc, M. A. Zwijnenburg, D. J. Adams and A. I. Cooper, *Angew. Chem. Int. Ed.*, 2016, **55**, 1792–1796.
- 3 R. S. Sprick, Y. Bai, A. A. Y. Guilbert, M. Zbiri, C. M. Aitchison, L. Wilbraham, Y. Yan, D. J. Woods, M. A. Zwijnenburg and A. I. Cooper, *Chem. Mater.*, 2019, **31**, 305–313.
- 4 P. Guiglion, C. Butchosa and M. A. Zwijnenburg, *J. Mater. Chem. A*, 2014, **2**, 11996–12004.
- 5 A. D. Becke, *Phys. Rev. A*, 1988, **38**, 3098–3100.
- 6 A. D. Becke, *J. Chem. Phys.*, 1993, **98**, 5648–5652.
- 7 P. J. Stephens, F. J. Devlin, C. F. Chabalowski and M. J. Frisch, *J. Phys. Chem.*, 1994, **98**, 11623–11627.
- 8 A. Schäfer, H. Horn and R. Ahlrichs, *J. Chem. Phys.*, 1992, **97**, 2571–2577.
- 9 A. Klamt and G. Schüürmann, *J. Chem. Soc., Perkin Trans. 2*, 1993, 799–805.
- 10 S. Hirata and M. Head-Gordon, *Chem. Phys. Lett.*, 1999, **314**, 291–299.
- 11 F. Furche, R. Ahlrichs, C. Hättig, W. Klopper, M. Sierka and F. Weigend, *Wiley Interdiscip. Rev. Comput. Mol. Sci.*, 2014, **4**, 91–100.
- 12 R. Ahlrichs, M. Bär, M. Häser, H. Horn and C. Kölmel, *Chem. Phys. Lett.*, 1989, **162**, 165–169.
- 13 M. Sachs, R. S. Sprick, D. Pearce, S. A. J. Hillman, A. Monti, A. A. Y. Guilbert, N. J. Brownbill, S. Dimitrov, X. Shi, F. Blanc, M. A. Zwijnenburg, J. Nelson, J. R. Durrant and A. I. Cooper, *Nat. Commun.*, 2018, **9**, 4968.
- 14 M. Sachs, E. Pastor, A. Kafizas and J. R. Durrant, *J. Phys. Chem. Lett.*, 2016, **7**, 3742–3746.
- 15 R. S. Sprick, M. Hoyos, M. S. Wrackmeyer, A. V. Sheridan Parry, I. M. Grace, C. Lambert, O. Navarro and M. L. Turner, *J. Mater. Chem. C*, 2014, **2**, 6520–6528.
- 16 P. Guiglion, C. Butchosa and M. A. Zwijnenburg, *J. Mater. Chem. A*, 2014, **2**, 11996–12004.
- 17 M. Sachs, R. S. Sprick, D. Pearce, S. A. J. Hillman, A. Monti, A. A. Y. Guilbert, N. J. Brownbill, S. Dimitrov, X. Shi, F. Blanc, M. A. Zwijnenburg, J. Nelson, J. R. Durrant and A. I. Cooper, *Nat. Commun.*, 2018, **9**, 4968.
- 18 Y. Bai, L. Wilbraham, B. J. Slater, M. A. Zwijnenburg, R. S. Sprick and A. I. Cooper, *J. Am. Chem. Soc.*, 2019, **141**, 9063–9071.
- 19 C. Yang, B. C. Ma, L. Zhang, S. Lin, S. Ghasimi, K. Landfester, K. A. I. Zhang and X. Wang, *Angew. Chem. Int. Ed.*, 2016, **55**, 9202–9206.
- 20 R. S. Sprick, Y. Bai, A. A. Y. Guilbert, M. Zbiri, C. M. Aitchison, L. Wilbraham, Y. Yan, D. J. Woods, M. A. Zwijnenburg and A. I. Cooper, *Chem. Mater.*, 2019, **31**, 305–313.
- 21 C. B. Meier, R. Clowes, E. Berardo, K. E. Jelfs, M. A. Zwijnenburg, R. S. Sprick and A. I. Cooper, *Chem. Mater.*, 2019, **31**, 8830–8838.
- 22 L. Li, Z. Cai, Q. Wu, W. Y. Lo, N. Zhang, L. X. Chen and L. Yu, *J. Am. Chem. Soc.*, 2016, **138**, 7681–7686.
- 23 L. Li and Z. Cai, *Polym. Chem.*, 2016, **7**, 4937–4943.

- 24 L. Guo, Y. Niu, S. Razzaque, B. Tan and S. Jin, *ACS Catal.*, 2019, **9**, 9438–9445.
- 25 K. Schwinghammer, S. Hug, M. B. Mesch, J. Senker and B. V. Lotsch, *Energy Environ. Sci.*, 2015, **8**, 3345–3353.
- 26 Y. S. Kochergin, D. Schwarz, A. Acharjya, A. Ichangi, R. Kulkarni, P. Eliášová, J. Vacek, J. Schmidt, A. Thomas and M. J. Bojdys, *Angew. Chem. Int. Ed.*, 2018, 14188–14192.
- 27 K. Schwinghammer, M. B. Mesch, V. Duppel, C. Ziegler, J. Senker and B. V. Lotsch, *J. Am. Chem. Soc.*, 2014, **136**, 1730–1733.
- 28 J. Kosco, M. Bidwell, H. Cha, T. Martin, C. T. Howells, M. Sachs, D. H. Anjum, S. Gonzalez Lopez, L. Zou, A. Wadsworth, W. Zhang, L. Zhang, J. Tellam, R. Sougrat, F. Laquai, D. M. DeLongchamp, J. R. Durrant and I. McCulloch, *Nat. Mater.*, 2020, DOI: 10.1038/s41563-019-0591-1.
- 29 D. J. Woods, R. S. Sprick, C. L. Smith, A. J. Cowan and A. I. Cooper, *Adv. Energy Mater.*, 2017, **7**, 1700479.